Supplementary Materials for

Disentangling water, ion and polymer dynamics in an anion exchange membrane.

Fabrizia Foglia[1*], Quentin Berrod[2], Gérard Gebel[2], Victoria García Sakai[3], Markus Appel[4], Jean-Marc Zanotti[5], Madhusudan Tyagi[6,7], Najet Mahmoudi[3], Adam J. Clancy[1], Thomas S. Miller[8], Keenan Smith[8], Daniel J. L. Brett[8], Paul R. Shearing[8], Sandrine Lyonnard[2*], Paul F. McMillan[1*]

This PDF file includes:
Supplementary Texts 1-3
Supplementary Figs. 1-20 and Tables 1-7
References (49 - 60)

Supplementary Text 1.
Water uptake and IEC

Fumasep FAD-55, as received in its Br^- ionomeric form, was soaked in NaCl solution (1.0 wt%) at *T* = 25 °C for 24 hrs and subsequently washed repetitively in ultrapure water to remove excess salt, tested by measuring the conductivity of the washing water. This pre-treatment, as indicated by the manufacturer [29], is necessary to ensure the specified degree of membrane expansion upon hydration.

The required chemical and isotopic contrasts for the neutron scattering experiments were then obtained by:

- hydrating the sample in its native form (Br^-) in D_2O (e.g immersing the membrane in 1 M NaBr solution at room temperature for 1 h followed by washing in D_2O): to produce the Br/D_2O sample;
- immersing the membrane in 1 M NaOH (aq) at room temperature for 1 h followed by washing in ultra-pure water to remove excess NaOH: this provided the OH/H_2O material;
- likewise, the membranes were treated in 1 M NaOD (aq) to achieve the OD/D_2O sample studied here.

1.1. Water uptake (λ)

Experiments were carried out on samples with a range of water contents, with hydration values (λ) expressed as the number of water molecules per functional group:

$$\lambda = mole_{H_2O}/IEC \cdot mole_{dry\ membrane} \quad (1)$$

in which IEC is the ion exchange capacity (meq g^{-1}). For FAD-55, in its Cl^- form, a value of ~2.0 meq g^{-1} is reported by the manufacturer [29].

Following exposure to a hydrating medium, experiments were carried out for membrane samples with water contents ranging between high (λ=13) to low (λ=3) hydration. Although the maximum water content of FAD-55 measured in this study is much lower than that reported as attainable by the manufacturer (i.e., 58 wt% [30]), our data agree with those reported by McGrath *et al.* who recorded a water uptake, in fully hydrated conditions, of ~28 wt% [31]. It is to be expected that membrane samples prepared by industrially established protocols to have nominally identical formulations might have some variation in nano- to mesoscale structure that might give rise to differences in total water uptake among samples available commercially, and hydrated or examined using local procedures.

The highest hydration level for samples examined here was obtained by first immersing the membrane in liquid water followed by gentle pad-drying to remove excess liquid; lower hydration values were obtained by removing the appropriate amount of water using a vacuum oven for specified times followed by weighing. Data were also recorded for fully dried samples obtained by heating overnight in a vacuum oven at *T*=40 °C.

1.2. Ion conductivity

In-plane OH^- and Cl^- conductivity of FAD samples (2.5x1 cm) held in a BekkTech four-point probe conductivity cell was determined using AC electrochemical impedance spectroscopy (EIS). Four equally spaced Pt electrodes, held in contact with the membrane, were connected to a frequency response analyser (Gamry, UK) with an oscillating voltage of 10 mV over a frequency range of 1 MHz – 1 Hz. The ion conductivity (σ; S cm^{-1}) of the membrane was obtained according to; $\sigma = l/RWt$, where l=0.425 cm is the fixed distance between the two inner Pt electrodes; R is the membrane resistance (Ω) corresponding to the low frequency X-intercept of the real axis in the Nyquist plot; W is the membrane width (cm) and t is the membrane thickness (cm). Humidity and temperature in the BekkTech cell was maintained by use of a Scribner Associates 850e test rig (Scribner, USA) with flowing N_2 gas at controlled temperature. EIS measurements were carried out with the membrane at a constant RH of 50-100% over a temperature range of 30-80 °C, allowing the membrane to equilibrate for at least 2 hours at each temperature step.

In Supplementary Figure 1 is reported the dependence of ion conductivity (σ) upon hydrating condition (relative humidity; RH%, and relative water uptake; λ) for FAD-55 membrane in OH- and Cl-form. No significant difference in conductivity was found at low hydration suggesting that the presence of OH^- has not caused any significant degradation to the ionomeric structure. In agreement with QENS data a clear change in conductivity was found above λ=7.

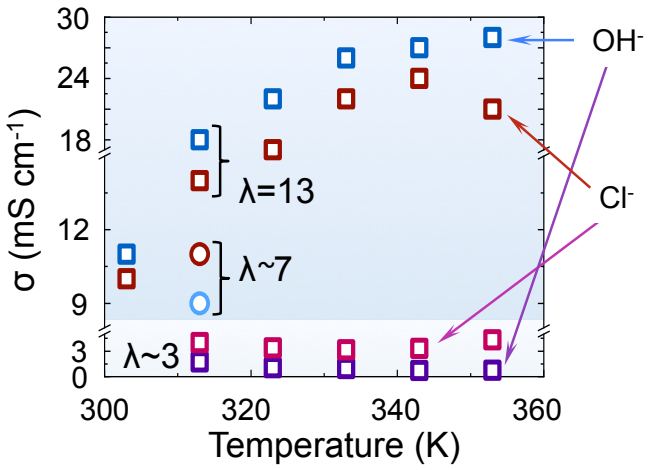

Supplementary Figure 1 | Temperature and water content dependence for ion conductivity. In the plot is reported the variation of ion (OH^- and Cl^-) conductivity as function of temperature and water uptake (λ). Data obtained at i) 100% relative humidity (RH; λ=13) are reported as blue and brown square symbols (OH^- and Cl^-; respectively); ii) at 80% RH (λ~7) are reported as blue and brown circles (OH^- and Cl^-; respectively) and iii) at 50% RH (λ~3) are reported as purple and pink square symbols (OH^- and Cl^-; respectively).

Supplementary Text 2.

Quasi-elastic neutron scattering (QENS) experiments

A typical QENS signal at a given momentum exchange (*Q*) is observed as a broadening in the energy transfer function as a consequence of local relaxational motions and/or diffusional events that involve centre-of-mass (*c-o-m*) translation. The time- and spatially-dependent scattering function, *S(Q,ω)*, contains information about the spatio-temporal correlation between identical nuclei (S_{inc}) and the static and dynamic correlations of distinct nuclei (S_{coh}) according to [49]:

$$S(Q,\omega) = S_{inc}(Q,\omega) + S_{coh}(Q,\omega) \quad (2)$$

where *S(Q,ω)* is the Fourier transform of the intermediate scattering function, *I(Q ,t)*:

$$S(Q,\omega) = \frac{1}{2\pi}\int_{+\infty}^{-\infty} I(Q,t)e^{-i\omega t}dt \quad (3)$$

The neutron scattering cross-sections for the nuclei considered in this study are (in barns): ^{1}H: σ_{inc}=80.27, σ_{coh}=1.76; ^{2}H (D): σ_{inc}=2.05, σ_{coh}=5.59; ^{79}Br: σ_{inc}=0.15; σ_{coh}=5.81; ^{81}Br: σ_{inc}=0.05; σ_{coh}=5.84. Because the AEM polymer dynamics are dominated by incoherent scattering contributions from ^{1}H covalently attached to the polymer backbone and its ionomeric functional groups, as are the OH^-/H_2O dynamics for samples hydrated with H_2O, and because of the low-*Q* range covered in the experiments, our analysis mainly focused on the incoherent scattering dynamics of the H-containing species. S_{inc} can be decoupled in terms of the vibrational, translational and rotational correlations of nuclei within the sample [49]:

$$S_{inc}(Q,\omega) = S_{vib}(Q,\omega) \otimes S_{rot}(Q,\omega) \otimes S_{trans}(Q,\omega) \otimes R \quad (4)$$

where *R* is the instrumental resolution function, determined experimentally using a vanadium (V) standard or from the sample at very low temperatures (~2-10 K), where all protons are expected to be frozen into quasi-static configurations that only contribute to elastic scattering for the accessible neutron spectrometer timescales.

For isotropic, harmonic vibrations expression (4) simplifies to:

$$S_{inc}(Q,\omega) = e^{-\frac{1}{3}Q^2\langle u^2\rangle}(S_{rot}(Q,\omega) \otimes S_{trans}(Q,\omega)) \quad (5)$$

where $\langle u^2 \rangle$ is the mean square displacement (msd) that accounts for both vibrational excitations, as well as proton delocalisation occurring on timescales faster than the instrument measurement window. “Immobile” protons, or those moving slower than the instrument resolution, are contained within the elastic scattering signal, *δ(ω)*, while very fast dynamics extending outside the measurement window give rise to an extremely broad signal that is modelled by an approximately flat background function, *B(Q)*.

To a very good approximation, the rotational and translational components in equation (5) can be modelled as independent Lorentzian functions. Depending on

the degree of localization of the dynamics probed for different types of motion and excitations, the relaxation lifetime measured as the inverse of the Lorentzian linewidth (Γ=half-width at half-maximum; HWHM) versus Q^2 relation shows (a) non-dispersive (polymer segmental relaxation, localized ion-hopping or H_2O reorientation/rotation motions) or (b) dispersive (i.e., centre-of-mass displacements of the scattering unit occur) signals. This difference in $\Gamma(Q^2)$ behavior is used to distinguish between different dynamic contributions to the QENS signal.

The QENS data here presented were acquired at four QENS spectrometers: i) IN6-Sharp (ILL, France); ii) IRIS (ISIS, UK) [46]; iii) IN16B (ILL, France) [47] and HFBS (NIST, USA) [48]. Raw data were normalized to the neutron flux and detector efficiency fluctuations against vanadium reference. The double differential cross section was then converted into the corresponding dynamic structure factor $S(Q,\omega)$. Data analysis were carried out directly on the $S(Q,\omega)$ spectra using Mantid [50], DAVE [51], or Origin 2019b.

2.1. Elastic – Inelastic Fixed Window Scan (EFWS – IFWS)

Fixed window scans provide an efficient tool to locate changes in dynamical behaviour as a function of Q or temperature (T) for a given instrument's accessible timescale. Dynamical signatures appear as changes in slope on the elastic (EFWS) intensity or slope changes and maxima in the inelastic intensity (IFWS). Assuming harmonic and isotropic vibrational oscillations, the temperature dependence of the msd is related to the EFWS intensity by:

$$\frac{I_{inc_{elastic}}(Q,T)}{I_{inc_{elastic}}(Q,T_{min})} = exp\left(-\frac{1}{3}Q^2\left(\langle u^2\rangle - \langle u^2\rangle_{T\_min}\right)\right) \quad (6)$$

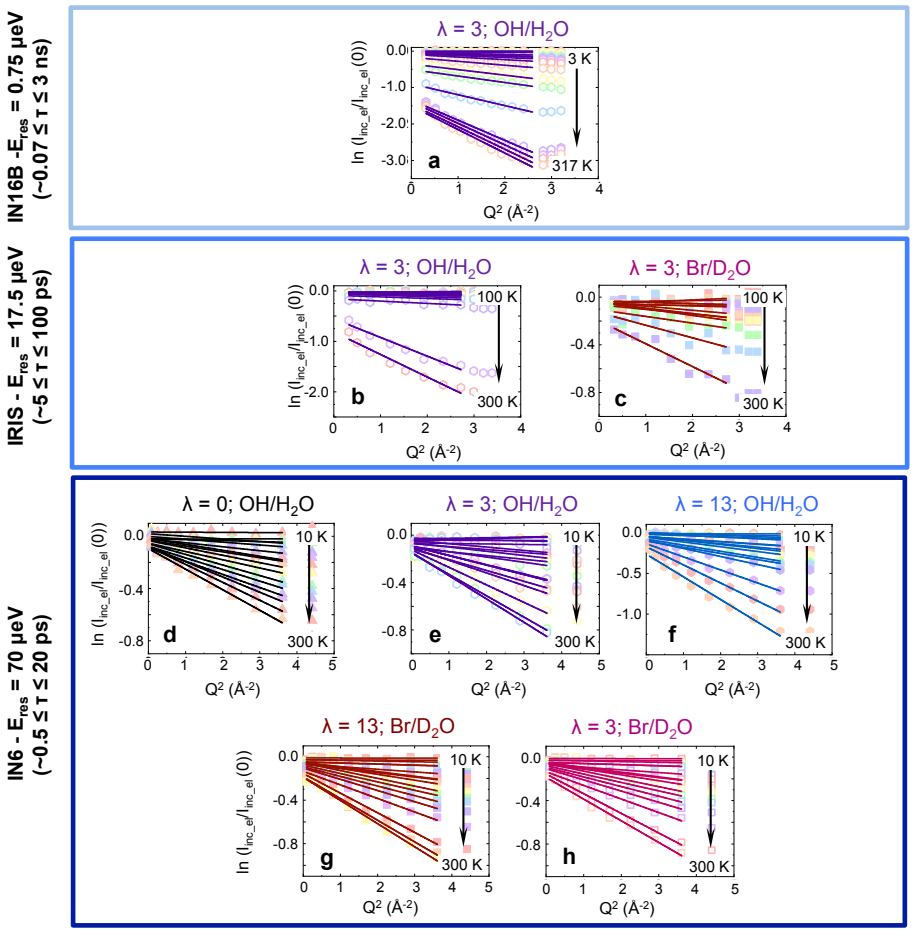

Supplementary Figure 2 | Mean Square Displacement. Fits used to evaluate the mean square displacement (<u^2>) with a restricted Q-range (up to ~1.6 Å^{-1}). **a**, Data for OH^-/H_2O at λ=3; E_{res}=0.75 μeV. **b**,**c**, Data at λ=3 for OH^-/H_2O (**b**) and Br^-/D_2O (**c**); E_{res}=17.5 μeV. **d-g**, Data for OH^-/H_2O at λ=0 (**d**), 3 (**e**) and 13 (**f**), as well as for Br^-/D_2O at λ=13 (**g**) and 3 (**h**); E_{res}=70 μeV.

Because of vibrational anharmonicity, the data deviate from the Debye-Waller approximation as T is increased, especially at higher Q. The onset of thermally activated localised hopping or diffusional dynamics also begins to contribute to <u^2> at higher temperature.

IFWS probes variations in dynamics leading to changes in the inelastic signal intensity, that reach a maximum when the QENS broadening matches ω_{off} (the energy offset determined by the chosen instrument parameters or selected during data analysis). Observations of the temperature variation in IFWS allow estimation of the activation energy (E_A) associated with the dynamic process [47]:

$$I_{\omega_{off}}^{IFWS}(T) \propto \frac{B}{\pi}\,(1 - A_0(Q))\,\frac{\tau(T)}{1+\omega_{off}^2\tau(T)^2} \tag{7}$$

$$\tau(T) = \tau_0 \exp\left(-\frac{E_A}{KT}\right) \tag{8}$$

$$T_{max} = \frac{E_A/KT}{\ln(1/\omega_{off}\tau_0)} \quad (9)$$

Here, B is a constant which accounts for the resolution function, τ is the relaxation time and τ_0 is its high temperature-limiting value, A_0 is the elastic incoherent structure factor (EISF) and K is the Boltzmann constant.

IFWS data were obtained by:

- setting the Doppler speed at IN16B, which allows following the evolution of the inelastic intensity at a defined energy (E-) transfer (BS spectrometer; Supplementary Fig. 3);

integrating the data over an arbitrarily selected E-range (TOF spectrometer; Supplementary Figs. 4-5). The integration width was chosen equivalent to E_{res}.

According to equations (7-9), applying different energy offsets leads to a temperature shift in the peak maximum as well as its intensity, and great attention needs to be paid in selecting ω_{off} for the data analysis. For TOF data recorded at IRIS, different ΔE ranges for integration were selected to begin disentangling dynamic contributions to the signal.

The data acquired at high resolution (IN16B; Supplementary Fig. 3a) for OH-form H_2O-hydrated at λ=3 show the existence of two dynamics associated to the activation of -CH_3 rotation (process 1; T~50 K) and the polymer side-chain relaxation (process 2). The inelastic signal, after reaching a maximum at T~260K, exhibits a pronounced decrease, as the process becomes too fast to be detected in this specific time window.

Probing the variation of inelastic intensity over a T-range by IFWS helps discriminate between local and diffusive motions, for which τ is either Q-independent or Q-dependent, respectively.

The analysis of the inelastic signal shows a clear Q-independence above Q=1.1 Å^{-1}, suggesting a localised motion (Supplementary Figs. 3b-c), with a slightly pronounced Q-dependency at $0.56 \leq Q \leq 1.1$ Å^{-1} (Supplementary Figs. 3b-c, insets). This latter suggests the presence of underlying diffusional dynamics, and it is supported by the activation energy E_A~23 kJ mol^{-1} (Supplementary Table 1), which is comparable with self-diffusion in supercooled bulk water [52].

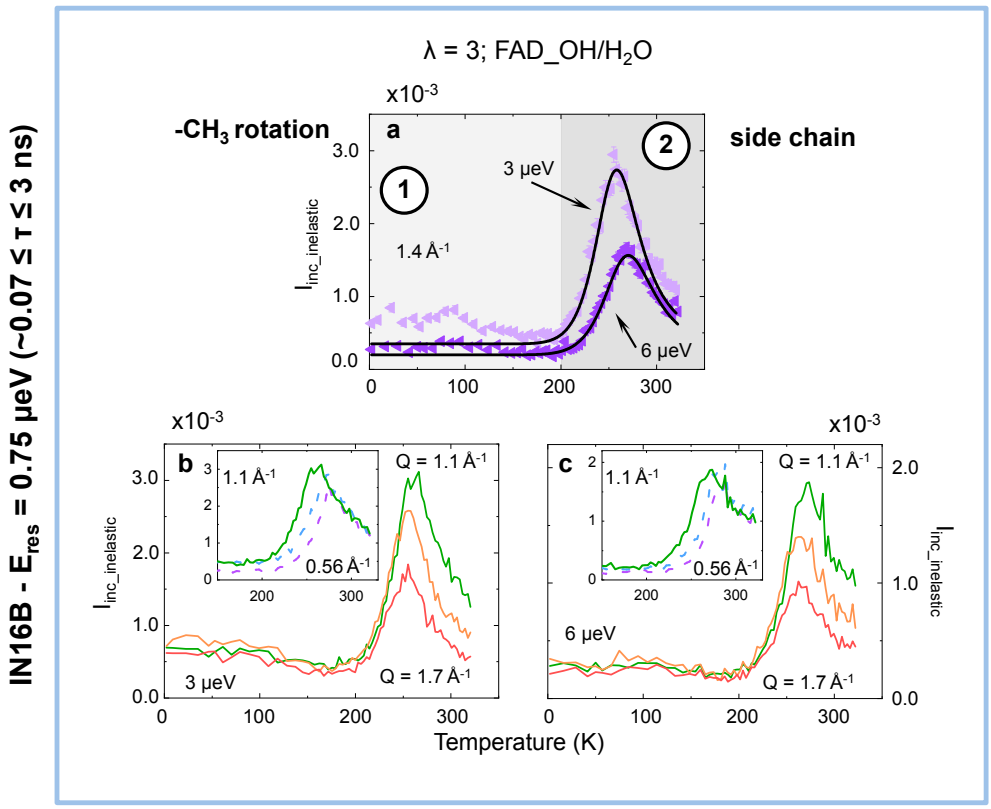

Supplementary Figure 3 | *Q*-dependence for IFWS at E_{res}=0.75 μeV. a, Inelastic fixed window scan (IFWS) for OH-form H_2O-hydrated at λ=3 and Q=1.4 Å^{-1} (E_{res}=0.75 μeV – IN16B; ILL). Data are obtained following the evolution of the inelastic intensity at a defined energy (E-) transfer and Doppler speed. **b**,**c**, *Q*-dependency of the inelastic signal at 3 and 6 μeV at 0.56≤*Q*≤1.70 Å^{-1} (**b**,**c**). The feature at low-T (~50 K) is associated to the activation of -CH_3 rotation (process 1). The signal centered at around 250 K is associated to the activation of the polymer side-chain relaxation (process 2). IFWSs show *Q*-dependent behavior only below 1.1 Å^{-1} (insets), suggesting a possible underlying diffusional process.

In the IRIS temporal window the data for OH-form H_2O-hydrated at λ=3 (Supplementary Figs. 4a-b; IRIS) clearly show the coupling of two dynamics: the polymer side-chain relaxation (process 2), and the water dynamics (process 3). More specifically, moving away from the elastic line, the data indicate a temperature shift and loss in IFWS peak intensity. This is not surprising, considering that at ~0.1 meV the scattering profile is dominated by water dynamics combined with polymer relaxation. As in the case of IN16B (Supplementary Fig. 3), a slightly pronounced *Q*-dependency is found at 0.56≤*Q*≤1.1 Å^{-1} (Supplementary Fig. 4c, insets), suggesting the presence of underlying diffusional dynamics (E_A~24 kJ mol^{-1}; Supplementary Table 1).

The coupling between process 2 and 3 is resolved investigating the Br-form D_2O-hydrated at λ=3 (Supplementary Figs. 4d-e; IRIS). In this specific case only the polymer side-chain relaxation (process 2) was detected, as the dynamics of D_2O is almost invisible. This latter is confirmed by the *Q*-independency of the signal (Supplementary Fig. 4f).

Supplementary Table 1: Msd drift ($d\langle u^2\rangle/dT$) and activation energies (E_A) computed from EFWS and IFWS. Data were modelled according to equations (6-9).

E_{res} (μeV)	Isotopic composition	Water uptake (λ)	$d\langle u^2\rangle/dT$ (Å^2 K^{-1})	E_A (kJ mol^{-1})
0.75	OH/H_2O	3	$7.7 \pm 0.8\ 10^{-4}$	23.0 ± 1.5
1.0	OH/H_2O	0	$8.3 \pm 0.7\ 10^{-4}$	-
		13	$10.9 \pm 0.8\ 10^{-4}$	-
17.5	OH/H_2O	3	$6.3 \pm 0.9\ 10^{-4}$	24.0 ± 2.1
	Br/D_2O			-
70	OH/H_2O	0		-
	&	3	$13.4 \pm 0.2\ 10^{-4}$	-
	Br/D_2O	13		-

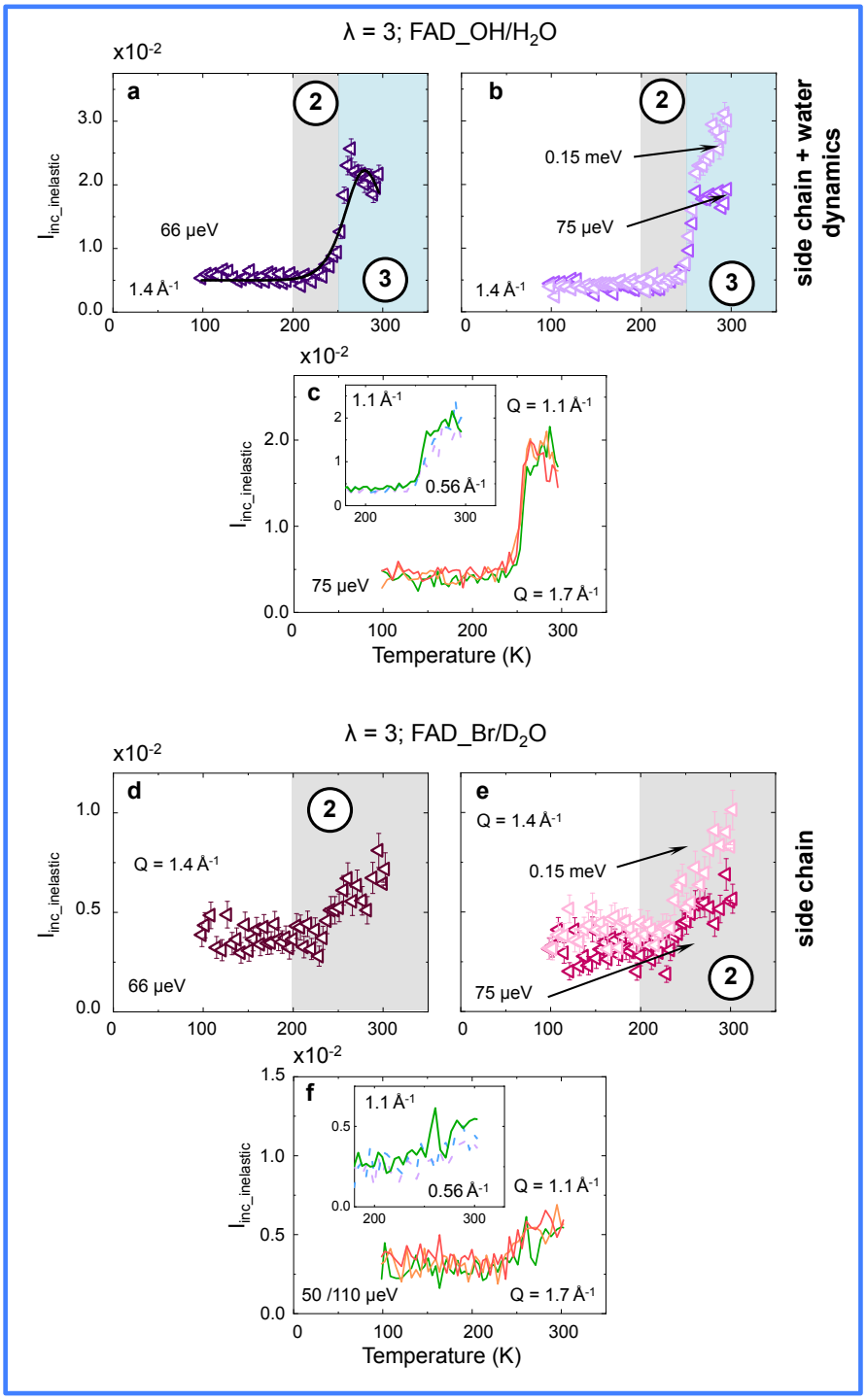

Supplementary Figure 4 | *Q*-dependence for IFWS at E_{res}=17.5 μeV. a-f, Inelastic fixed window scan (IFWS) for OH-form H_2O-hydrated (**a-c**) and in Br-form D_2O-hydrated (**d-f**) at λ=3 and Q=1.4 Å^{-1}. Data are obtained integrating the inelastic signal over different energy intervals centered at: i) 66; ii) 75 μeV and iii) 0.15 meV (E_{res}=17.5 μeV – IRIS; ISIS). In the H_2O-hydrated contrast (**a-c**) the variation in inelastic intensity is associated to the coupling between polymer side-chain relaxation (process 2, 200≤T≤250 K) and water dynamics (process 3, T>250 K). The Q-dependence of the signal is investigated at 0.56≤Q≤1.70 Å^{-1}. The presence of the water dynamics is responsible for the Q-dependent behavior below 1.1 Å^{-1} (inset panel **c**). Note here that, despite being not really defined the Q-independence, it was already saw (more convincingly) on IN16B data (see Supporting Fig. 3). In the D_2O-hydrated contrast (**d-f**) the variation in inelastic intensity is associated only to the polymer side-chain relaxation (process 2, 200≤T≤250 K), as confirmed by the Q-independency of the signal all over the investigated Q-range (**f**).

IN6-Sharp data (Supplementary Figs. 5a-b) show similar outcome as IRIS. In this specific temporal window the H_2O-hydrated samples at $3 \leq \lambda \leq 13$ indicates the coupling between: i) the activation of $-CH_3$ rotation (process 1; T~50 K), the polymer side-chain relaxation (process 2), and the water dynamics (process 3). The latter is clearly visible also by the Q-dependency of the signal (H_2O-hydrated at λ=13; Supplementary Figs. 5c-d). The variation in water uptake, in the H_2O-hydrated samples, determines the reduction in intensity at high-T (blue line; λ=13, and purple line; λ=3) as well as the variation in Q-dependency of the signal (Q-dependent *vs* Q-independent at λ=13 and 3, respectively; Supplementary Figs. 5c-e). It has to be notice here, however, that the Q-independency of the inelastic intensity for H2O-hydrated at λ=3, in this spectroscopic window is mainly due to the polymer relaxation, as water dynamics is too slow (almost included to the elastic line of IN6-Sharp). Indeed the investigation of the D_2O-hydrated sample at λ=13, show similar behavior (brown line in Supplementary Fig. 5c and Supplementary Fig. 5f). The signal associated to the water dynamics disappear in the dry (black line; Supplementary Fig. 5g) and D_2O-hydrated at λ=3 (pink line; Supplementary Fig. 5g) samples, where is only found the coupling between the activation of $-CH_3$ rotation (process 1; T~50 K), and the polymer side-chain relaxation (process 2).

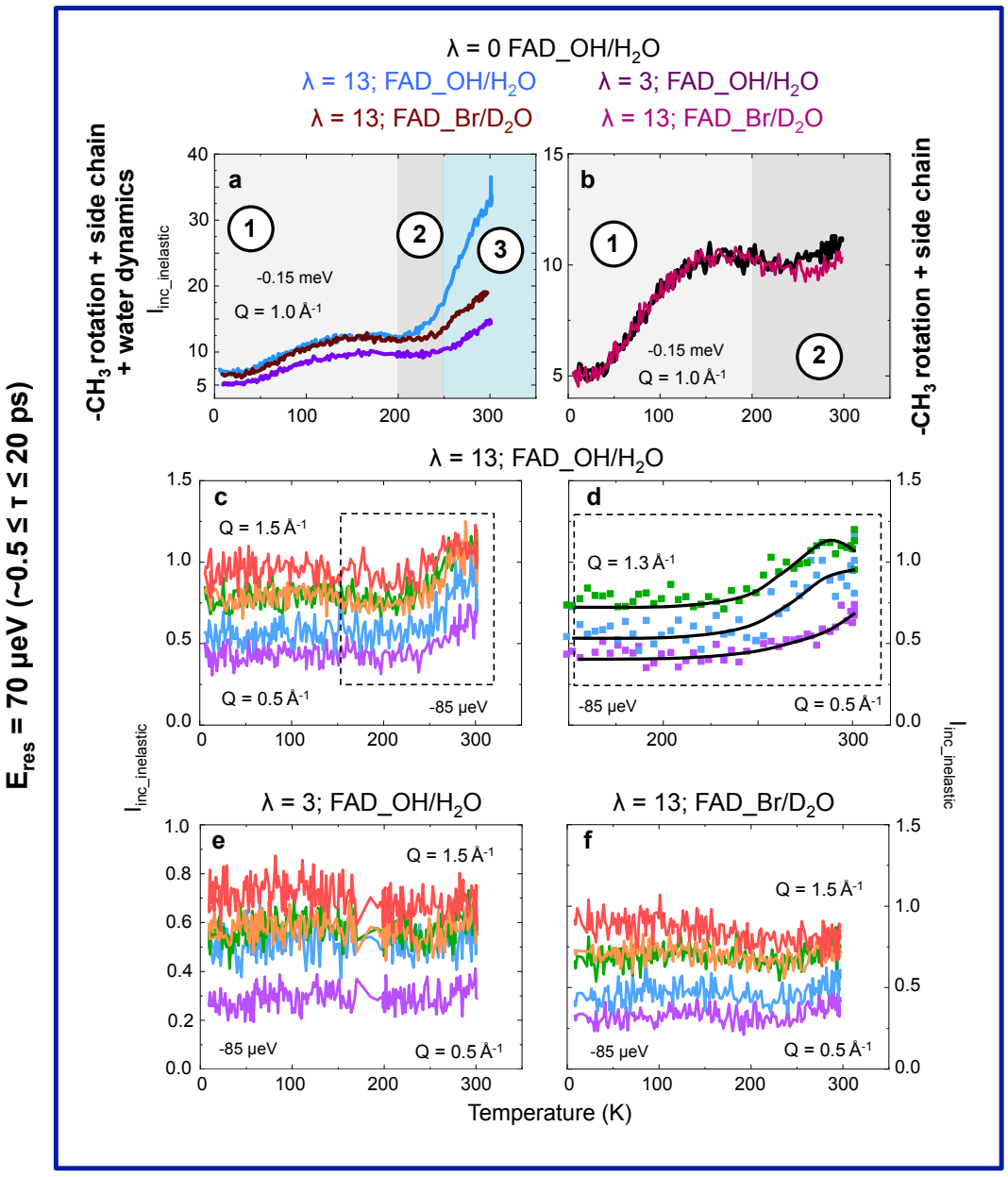

Supplementary Figure 5 | *Q*-dependence for IFWS at E_{res}=70 μeV. a-f, Inelastic fixed window scan (IFWS) for OH-form H_2O-hydrated and in Br-form D_2O-hydrated at 0≤λ≤13 and E_{res}=70 μeV (IN6-Sharp; ILL). Data are obtained integrating the inelastic signal over different energy intervals centered at: i) -0.15 meV (Q=1.0 Å^{-1}; **a**-**b**) and ii) -85 μeV (0.5≤Q≤1.5 Å^{-1}; **c**-**f**). In the H_2O-hydrated contrast at λ=13 (blue line, **a**) the variation in inelastic intensity is associated to the coupling between to the activation of -CH_3 rotation (process 1), the polymer side-chain relaxation (process 2, 200≤T≤250 K) and water dynamics (process 3, T>250 K). The presence of water dynamics is confirmed by the Q-dependence of the signal (**c**-**d**). Panel **f** represents a highlight to show the Q-dependency; lines are guides to the eye. As the hydrating medium is changed to D_2O (at λ=13 – brown line, **a**) the variation in inelastic intensity the intensity associated to the isotopic variation. Similar the H_2O-hydrated contrast at λ=3 (purple line, **a**) where the signal is Q-independence of the signal (**e**). In dry conditions (λ=0 – black line, **b**), as well as at low-hydration in D_2O (λ=3 – pink line, **b**) the variation in inelastic intensity is associated to the coupling between to the activation of -CH_3 rotation (process 1) and the polymer side-chain relaxation (process 2, 200≤T≤250 K), as supported by the Q-independency of the signal (**f**).

2.2. S(*Q, ω*) datasets and fitting

QENS data contain different contributions to the relaxation dynamics operating over different timescales. The analysis usually requires multi-Lorentzian components, whose width and intensity inform on the nature of the dynamics (e.g. local *vs* diffusive motions; *Q*-independent *vs* -dependent, respectively).

The analysis of the experimental *S(Q,ω)* require to convolute the instrumental resolution to a well-selected theoretical *S(Q,ω)*, i.e. assume a model for each type of motions expected to take place in the material. One major difficulty is that components may overlap, which often limit QENS data interpretation and does not allow discriminating unambiguously different scenarii. To insure the uniqueness and reliability of the analysis, the same analytical correlation function must be used to describe the dynamics across the extended range of timescales, where the weight of the various components will be tuned depending on the dynamic window (e.g. a given component will be "hidden" in the elastic peak -too slow to be resolved- or appearing as "flat background" -too fast). Moreover, playing with membrane hydration and temperature conditions allow to add constraints on the chosen models as the full set of data has to be consistently analysed over the whole *Q*- and time-scale range.

Here we applied such cross-correlated analysis, resulting in the treatment of ~400 spectra using the same formalism (see Supporting Texts 2.2-2.5 for details). This approach allowed to consistently reproducing the entire datasets as well as detailing these multi-scale dynamical processes

All plots representing the scattering profile analyses (*S(Q,ω) vs ΔE*) comprise the following components:

- Elastic contribution (delta function convoluted with the instrumental resolution function) obtained from the sample at ~2 K; blue line.
- Polymer contribution (*Q*-independent component); grey line.
- Water diffusion (*Q*-dependent component; $\lambda \geq 7$); dark blue line (where present).
- Water localised motion (*Q*-independent component; $3 \leq \lambda \leq 5$); light blue line (where present).
- Ion-hopping (*Q*-independent component); purple line (where present).
- Flat background (accounting for vibrational excitations much faster than the observational timescale); black dashed line (where present).
- The global fit is represented as red continuous curve.
- Data points are presented as black symbols.

* At high-energy resolution (IN16B) polymer and water dynamics are coupled (having similar width), therefore in the plots this component is reported either in light (λ=3) or in dark (λ=13) blue.

** This colour coding applies to the plots presented below, with different intensities associated with each probed timescale.

The analysis (in E-space) of OH-form at 0≤*λ*≤13 samples, acquired at high-resolution (IN16B; ILL), allows characterizing most of the dynamics within the system.

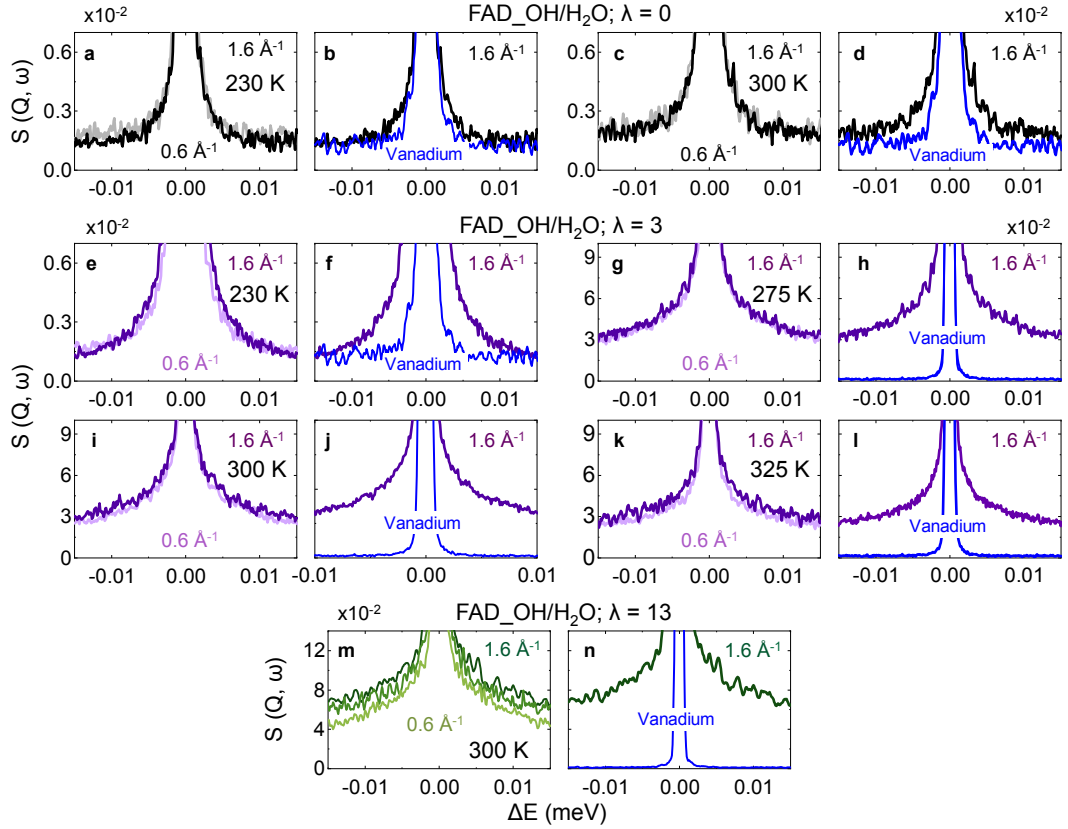

Supplementary Figure 6 | Q-dependence and comparison against Vanadium for FAD-55 (H_2O- and D_2O-hydrated) at 0≤*λ*≤13; E_{res}=0.75 μeV. a-d, OH-form, dry (*λ*=0), at 230 and 300 K; *Q*=0.6 and 1.6 Å^{-1}. **e-l**, OH-form, H_2O-hydrated (*λ*=3), between 230 and 325 K; *Q*=0.6 and 1.6 Å^{-1}. **m-p**, OH-form, H_2O-hydrated (*λ*=13), at 300 K; *Q*=0.6, 1.3 and 1.6 Å^{-1}. **o-p**, Br-form, D_2O-hydrated (*λ*=13), at 300 K; *Q*=0.6 and 1.6 Å^{-1}.

The *Q*-dependence and comparisons against vanadium, at high resolution (E_{res}=0.75 μeV), reveals that QENS broadening in the dry sample is activated above 230 K and is associated with a localised (*Q*-independent) motion (Supplementary Figs. 6a-d).

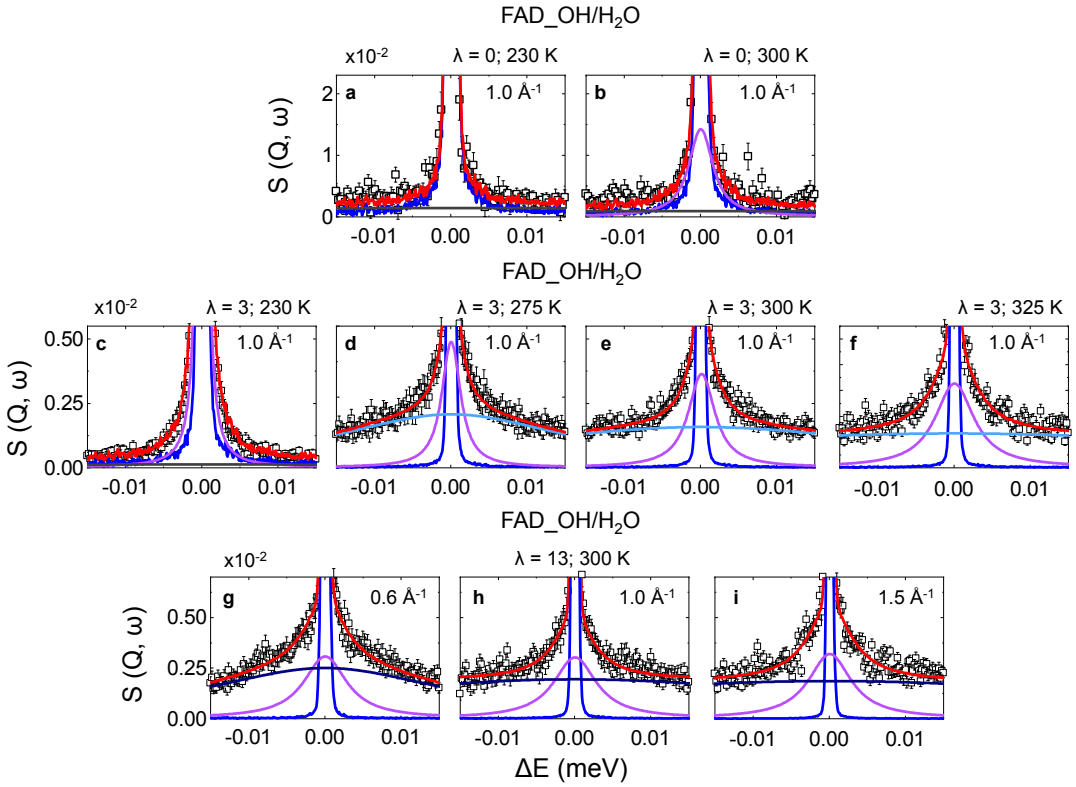

Supplementary Figure 7 | QENS profiles for FAD-55 H_2O-hydrated at 0≤λ≤13; E_{res}=0.75 μeV. a-i, Profiles recorded for dry (λ=0) sample in OH-form, H_2O-dydrated, at: i) λ=0 (230 and 300 K; Q=1.0 Å^{-1}; **a**-**b**); ii) λ=3 (from 230 to 325 K; *Q* = 1.0 Å^{-1}; **c**-**f**) and at iii) λ=13 (300 K; *Q*=0.6, 1.0 and 1.5 Å^{-1}; **g**-**i**). In this time window polymer and water dynamics are coupled (having similar width), therefore in the plots this component is reported either in light (λ=3) or dark (λ=13) blue. OH^- hopping is reported as purple line.

Based on the dynamics show in the FWS profile for the dry sample (Fig. 2a-b, main paper), the analysis of the scattering profiles in E-domain at 230 K are modeled only accounting for the polymer dynamics (grey line; Supplementary Fig. 7a). Increasing the temperature to 300 K, as revealed by the comparison of raw data against Vanadium standard (Supplementary Fig. 6d), an extra Lorentzian function is required to model the data. This process (purple line; Supplementary Fig. 7b) was found to be *Q*-independent and associated with OH^- hopping.

These two distinct components are also seen in the H_2O-hydrated sample (λ=3). At low-hydration (λ=3; H_2O-hydrated) the scattering profiles were modelled accounting for OH^- hopping (purple line; Supplementary Figs. 7c-f), and a further Lorentzian function, which in this specific case is associated to the coupling between side chain relaxation and dynamics of water trapped within the polymer matrix (light blue line; Supplementary Figs. 7c-f). The data indicate that only *Q*-independent motions are detectable throughout the investigated *T*-range (Supplementary Figs. 6e-l). However the slightly pronounced *Q*-dependence of the EFWS (Supplementary Fig. 3c, insets) found at low-*Q*, suggests that at this hydration level the water is nanoconfined.

Similarly, at higher hydration (e.g. λ=13) the data were modelled accounting for OH^- hopping (purple line; Supplementary Figs. 7g-h), and a further Lorentzian function,

which in this specific case is associated to the coupling between side chain relaxation and dynamics of water diffusing within the polymer matrix (dark blue line; Supplementary Figs. 7g-h). This latter is responsible for the *Q*-dependency of the signal (Supplementary Fig. 6m). Similar outcome was also fund while analyzing HFBS data (Supplementary Fig. 8).

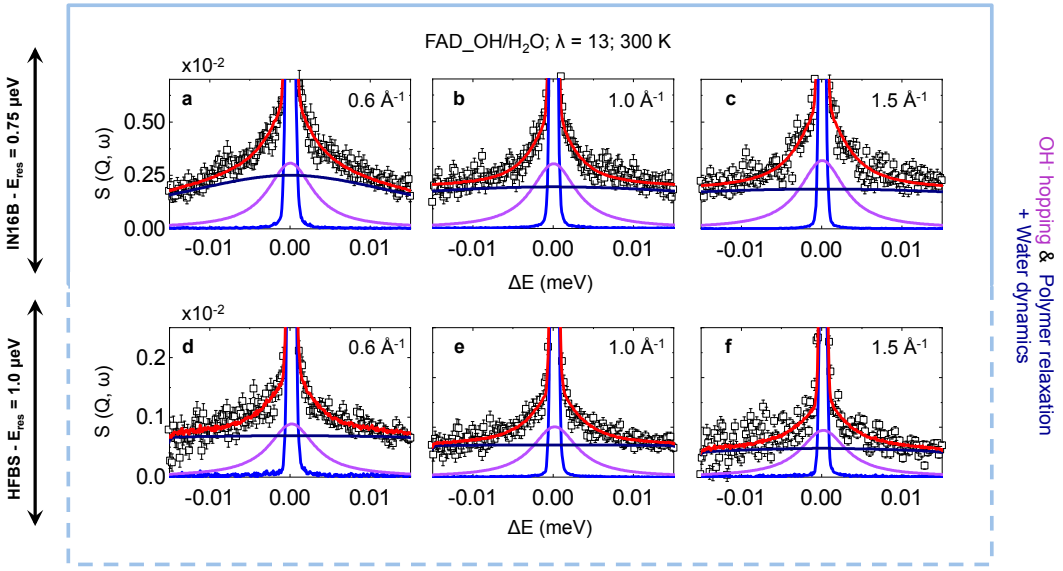

Supplementary Figure 8 | QENS profiles for FAD-55 H_2O-hydrated at *λ*=13; E_{res}=0.75 and 1.0 μeV. a-f, Profiles acquired using IN16B (**a**-**c**; E_{res}=0.75 μeV) and HFBS spectrometer (**d**-**f**; E_{res}=1.0 μeV). FAD samples were investigated fully hydrated (λ=13) in OH-form, H_2O-dydrated, at 300 K. In the plots have been presented three representative *Q*-values: Q=0.6, 1.0 and 1.5 $Å^{-1}$. OH^- hopping is reported as purple line; polymer and water dynamics are coupled (having similar width), therefore in the plots this component is reported in dark blue.

Upon investigation with faster probe timescales, the ion-hopping feature associated with slow dynamics is no longer visible, as it becomes convoluted with the elastic line (Supplementary Figs. 9, 12; IRIS and IN6 data, respectively). Based on the dynamics observed from the EFWS (Supplementary Fig. 4), the data for λ=0 and in the D_2O-hydrated sample are modeled by accounting only for polymer side chain relaxations (grey line; Supplementary Figs. 9a-i, 10a-f and 11a).

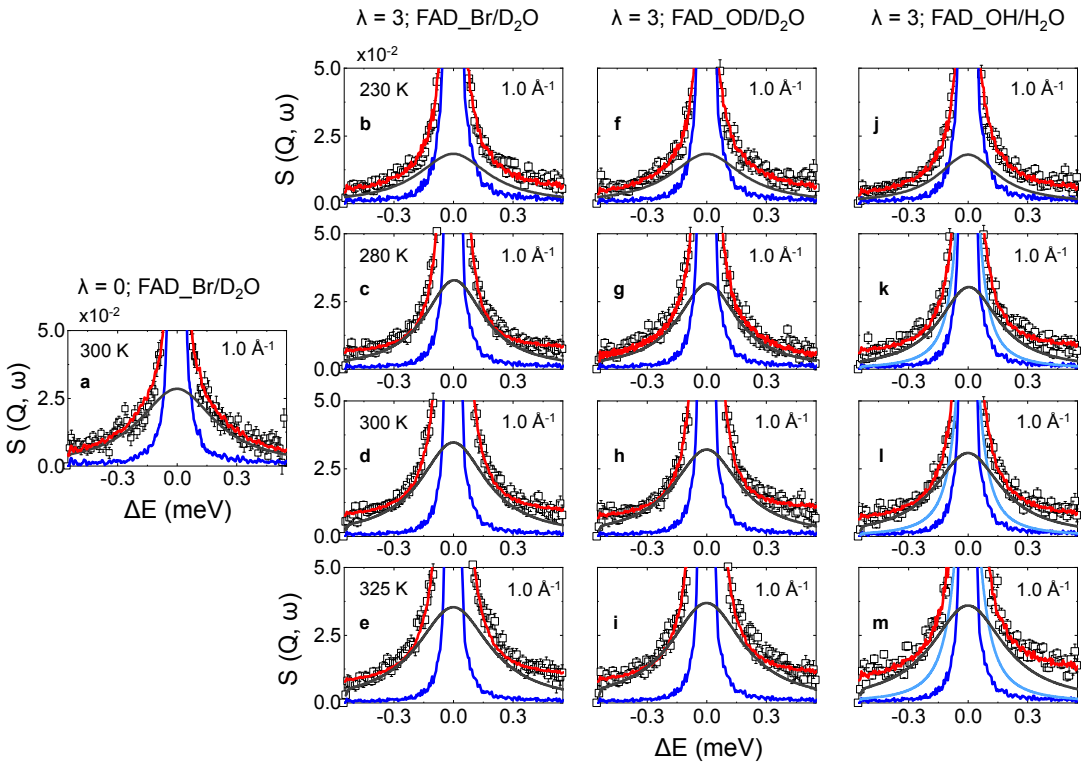

Supplementary Figure 9 | QENS profiles for FAD-55 acquired at both (H_2O- and D_2O-hydrated) at λ=0 and 3; E_{res}=17.5 μeV. a, Profile recorded for Br-form, D_2O-hydrated, dry (λ=0) at 300 K; Q=1.0 $Å^{-1}$. **b**-**e**, Br-form, D_2O-hydrated (λ=3), from 230 to 325 K; Q=1.0 $Å^{-1}$. **f**-**i**, OD-form, D_2O-hydrated (λ=3), from 230 to 325 K; Q=1.0 $Å^{-1}$. **j**-**m**, OH-form, H_2O-hydrated (λ=3), from 230 to 325 K; Q=1.0 $Å^{-1}$.

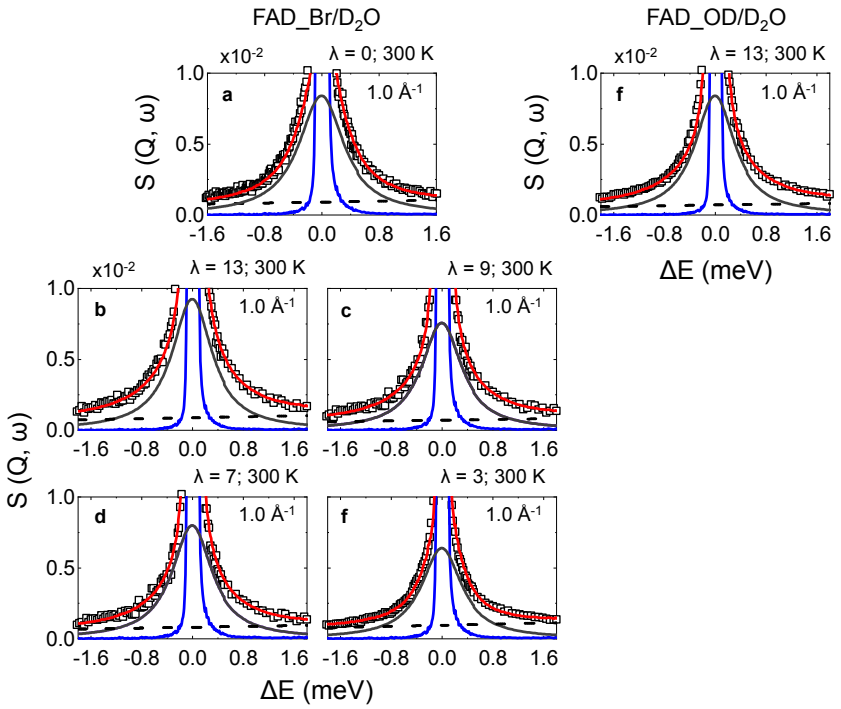

Supplementary Figure 10 | QENS profiles for FAD-55 D_2O-hydrated at 300 K and 0≤λ≤13; E_{res}=70 µeV. a, Profile for Br-form dry (λ=0), at 300 K; Q=1.0 Å^{-1}. **b**-**c**, Br-form, D_2O-hydrated (λ=13 to 3), at 300 K; Q=1.0 Å^{-1}. **f**, OD-form, D_2O-hydrated (λ=13), at 300 K; Q=1.0 Å^{-1}.

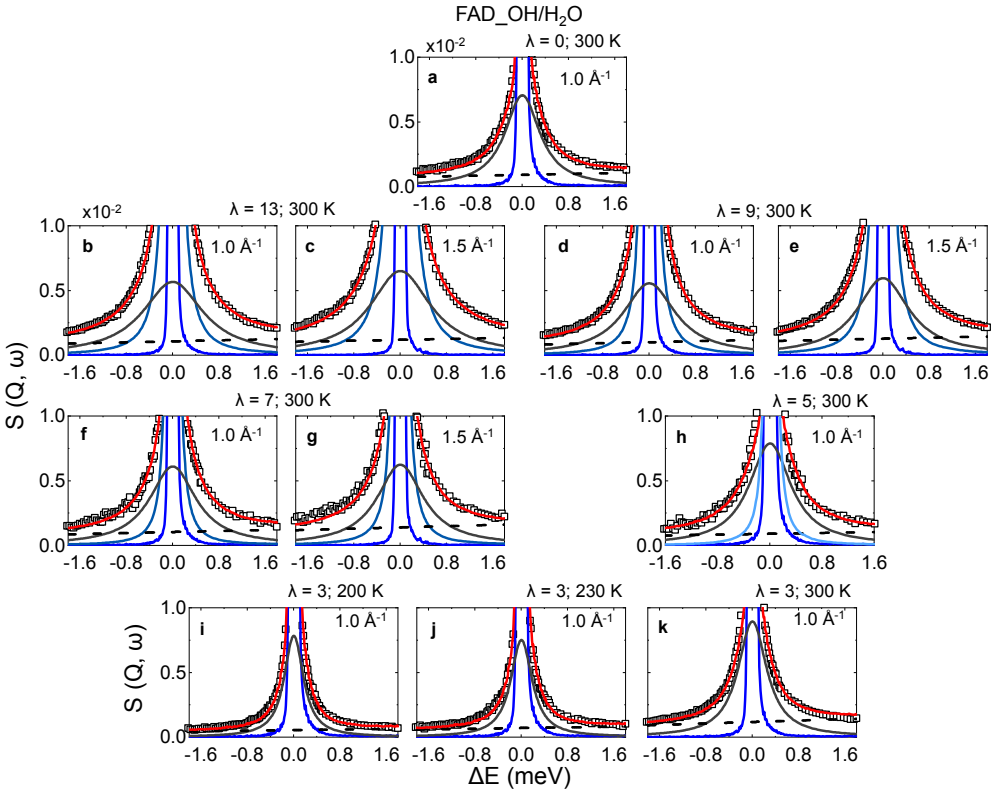

Supplementary Figure 11 | QENS profiles for FAD-55 H_2O-hydrated at 0≤λ≤13; E_{res}=70 µeV. a, Profile for OH-form dry (λ=0), at 300 K; Q=1.0 Å^{-1}. **b**-**g**, OH-form, H_2O-hydrated, at λ=13 (**b**-**c**), 9 (**d**-**e**) and 7 (**f**-**g**); 300 K; Q=1.0 and 1.5 Å^{-1}. **h**-**k**, OH-form, H_2O-hydrated, at λ=5 (300 K; **h**) and 3 (from 200 to 300 K; **i**-**k**); Q=1.0 Å^{-1}.

When H_2O-hydrated, however, the scattering profile also contains the dynamics of water trapped within the membrane matrix, as suggested by the slight *Q*-dependence at low-*Q* (Supplementary Fig. 3c). However, as this dynamics is quite slow at λ=3, it is only visible on IRIS time-scale (Supplementary Figs. 9j-m), while on IN6-Sharp it emerges above λ=5 (Supplementary Fig. 11). This coupling is disentangled within the IRIS time-scale as shown in Supplementary Figure 10, where a single component in IN16B (light blue line in panels a and b), translates into two separate contributions (grey -polymer relaxation- and light blue -water dynamics- lines in panel c) at lower energy resolution. The presence of water dynamics is clearly visible in the scattering profile obtained by removing the polymer contribution (from the full scattering patter (OH/H_2O – OD/D_2O; Supplementary Figs. 12g-i).

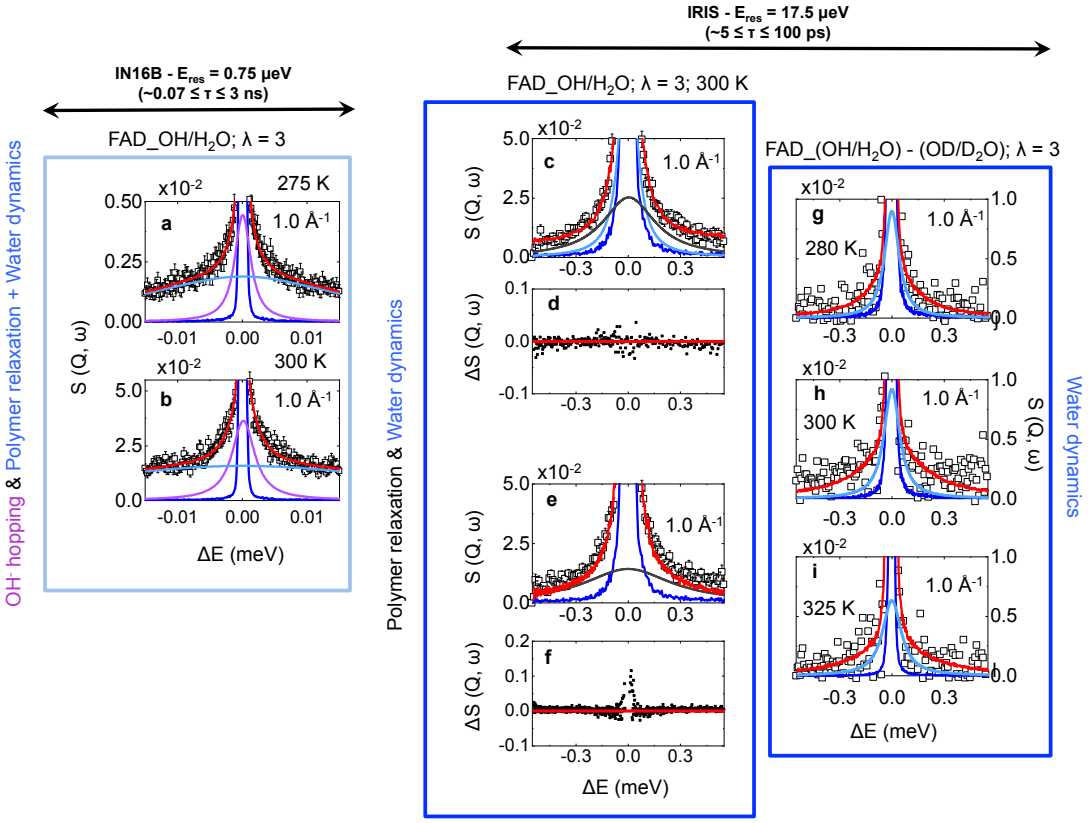

Supplementary Figure 12 | Fitting model using one *vs* two Lorentzian functions for FAD-55, OH-form, at λ=0 and 3; E_{res}=0.75 and 17.5 μeV. a,**d**, OH-form, H_2O-hydrated (λ=3; E_{res}=0.75 μeV), at 275 and 300 K; *Q*=1.0 $Å^{-1}$. Analysis was performed using two Lorentzian functions (for OH-hopping and polymer relaxation coupled to water dynamics; purple and light blue lines, respectively). **c**-**f**, OH-form, H_2O-hydrated (λ=3; E_{res}=17.5 μeV), at 300 K; *Q*=1.0 $Å^{-1}$. Analysis was performed using either two (polymer relaxation and water dynamics; grey and light blue lines, respectively) or only one (polymer relaxation; grey line) Lorentzian function. Plot showing the difference between data points and fitting profile are reported in d and f. **g**-**i**, Contrast highlighting the water dynamics (OH/H_2O – OD/D_2O; E_{res}=17.5 μeV), obtained by removing the polymer contribution (OD-form, D_2O-hydrated) from the sample in OH-form (H_2O-hydrated, λ=3), 280≤*T*≤325 K; *Q*=1.0 $Å^{-1}$.

2.3. Non-dispersive QENS signals

2.3.1. Relaxation time and ion-hopping distance

The relaxation time (τ_R) associated with a spatially localized process is calculated as [49]:

$$\tau_R = {\hbar}/{\Gamma} \tag{10}$$

and the intensity of the *Q*-independent ion-hopping signal is modelled by [23]:

$$\mathrm{I}_{hopping} = 1 - \exp\left(-Q^2\sigma^2\right) \tag{11}$$

where 2σ represents the mean hopping distance.

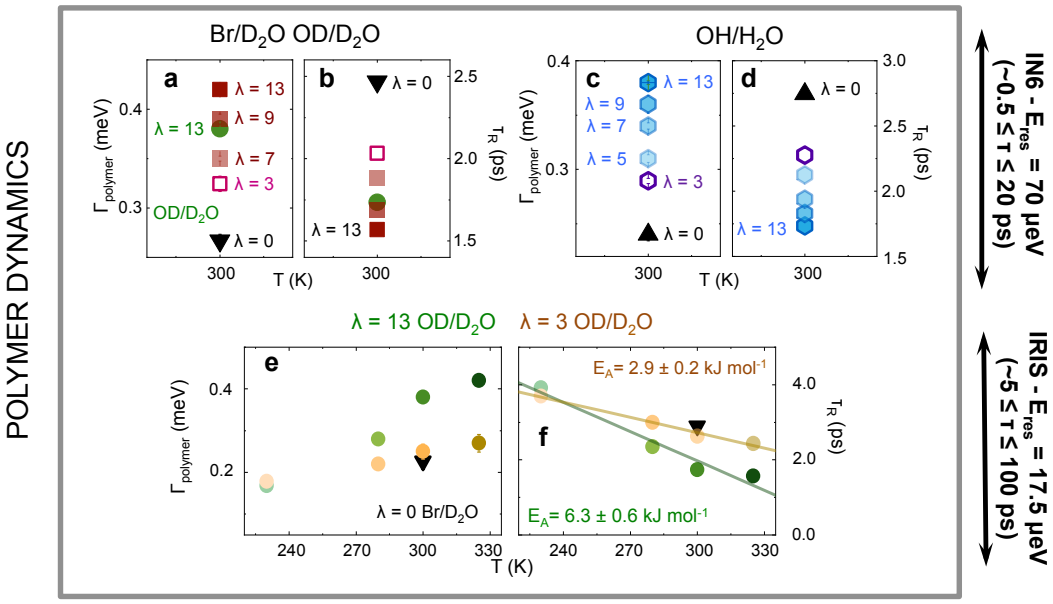

Supplementary Figure 13 | HWHM (*Γ*) and relaxation time FAD-55 (H_2O- and D_2O-hydrated), at 0≤*λ*≤13. a-d, Data acquired at E_{res}=70 μeV. **e,f**, Data acquired at E_{res}=17.5 μeV. Samples at λ=0 are presented as black symbols; OH-form, H_2O-hydrated, are reported in blue (λ=13) and purple (λ=3); OD-form, D_2O-hydrated are reported in green (λ=13) and orange (λ=3) and Br-form, D_2O-hydrated are reported in brown (λ=13) and pink (λ=3).

Supplementary Table 2: Dynamical parameters associated to polymer relaxation, computed according to equation (10). The relaxation times for the polymer dynamics for the H_2O-hydrated samples (at E_{res}=17.5 μeV) have been constrained to the values obtained analysing D_2O-hydrated samples.

E_{res} (μeV)	λ	T (K)	τ (ps)	
			D_2O-hydrated	H_2O-hydrated
17.5	0	300	2.90 ± 0.25	
	3	230	3.81 ± 0.29	
		280	3.00 ± 0.18	
		300	2.64 ± 0.19	
		325	2.44 ± 0.19	
	13	230	4.00 ± 0.31	
		280	2.35 ± 0.09	
		300	1.73 ± 0.07	
		325	1.57 ± 0.05	
70	0	300	2.47 ± 0.15	2.74 ± 0.16
	3	200	-	3.51 ± 0.21
		230	-	3.14 ± 0.19
		300	2.03 ± 0.09	2.28 ± 0.13
	5	300	-	2.14 ± 0.12
	7		1.88 ± 0.13	1.94 ± 0.11
	9		1.68 ± 0.11	1.83 ± 0.12
	13		1.64 ± 0.09	1.73 ± 0.11

Supplementary Table 3: Dynamical parameters associated to OH^- hopping, computed according to equations (10-11).

E_{res} (μeV)	λ	T (K)	Composition	τ (ps)	σ (Å)
0.75	0	230	OH/H_2O	-	-
		300		380.2 ± 67.0	1.79 ± 0.09
	3	230		439.3 ± 83.4	1.81 ± 0.08
		275		315.3 ± 53.5	2.16 ± 0.12
		300		274.6 ± 40.0	2.62 ± 0.09
		325		235.3 ± 24.4	2.80 ± 0.13
	13	300		199.7 ± 21.1	2.96 ± 0.12

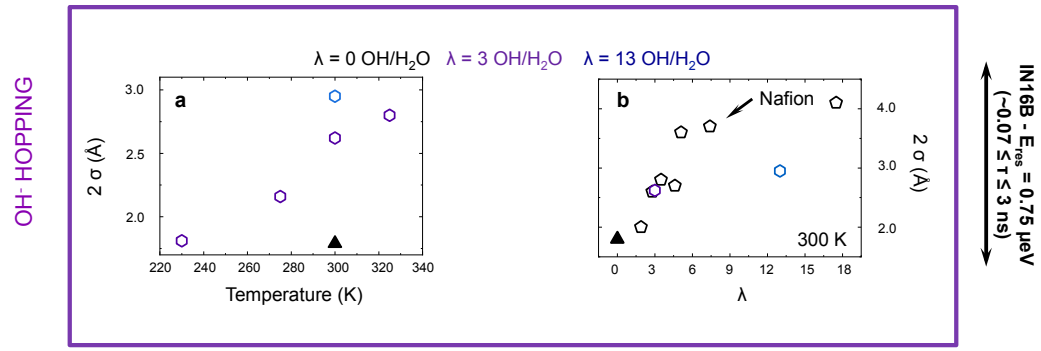

Supplementary Figure 14 | Variation of the hopping length as a function of temperature or water uptake. a,**b**, Data obtained by the analysis of high resolution BS spectrometer (E_{res}=0.75 μeV); in this configuration only hopping is visible. Data related to Nafion are presented as empty black symbols [23] (**b**).

Supplementary Table 4: Activation energy (E_A) for both polymer relaxation and ion hopping. Data were modelled according equation (8).

E_{res} (μeV)	Composition	λ	Movement	E_A (kJ mol^{-1})
0.75	OH/H_2O	3	OH^- hopping	4.0 ± 0.2
17.5	OH/H_2O	3	Polymer relaxation	2.9 ± 0.2
	OH/H_2O	13		6.3 ± 0.6

2.3.2. Elastic Incoherent Structure Factor (EISF)

QENS experiments investigate translational and/or rotational movements by mainly accounting for the incoherent scattering function, $S_{inc}(Q,\omega)$ (equation (5)). This quantity contains not only information about the relaxation dynamics of protons (i.e. the quasielastic component) but also their relative spatial arrangement within the instrumental time resolution (i.e., the elastic component to the scattering). Therefore, in the case of rotational or confined translational movements, $S_{inc}(Q,\omega)$ can be rewritten as:

$$S_{inc}(Q,\omega) = A_0(Q,T)\delta(\omega) + \big(1 - A_0(Q,T)\big)L(Q,T,\omega) \quad (12)$$

where $A_0(Q,T)$ is the EISF, $\delta(\omega)$ is the Dirac delta function representing the elastic peak and $L(Q,T,\omega)$ is a spectral function.

The EISF is computed as a ratio between elastic intensity over total intensity, and is modelled according to the possible motions in the system; therefore great care needs to be given to the model used especially in the case of mixtures (e.g. hydrated membrane systems) containing different contributions to the dynamical properties. Note here that EISF is only modelled in the case of *Q*-independent signal.

In the present case, based on the membrane chemistry considered: i) jumps among three equivalent sites, to account for CH_3 rotation in the polymer matrix (equation (13a); for D_2O-hydrated samples) and ii) free rotation, to model OH^- hopping within the polymer matrix (equation (13b); for H_2O-hydrated samples at high resolution) [49]:

$$A_{0\_CH_3} = x + (1-x)\left\{\frac{1}{3}\left[1 + 2j_0(Qr\sqrt{3})\right]\right\} \quad (13a)$$

$$A_{0\_hopping} = y + (1-y)(j_0^2(Qr)) \quad (13b)$$

Here j_0 is the Bessel function of the zeroth order, r is the radius (1.1 Å for CH_3 and 0.98 Å for OH^-), x and y are the fraction of immobile protons in the system, while Φ_P and Φ_W are the fraction of polymer (CH_3) and water (OH^-) in the mixture calculated from the water uptake (λ).

Not unexpectedly, upon increasing temperature and swelling the analysis of EISF suggests that the system get more mobile. Furthermore samples in the dry and low-hydration show no difference in percentage of mobile species between Br- and OH-/OD-form, indicating no degradation.

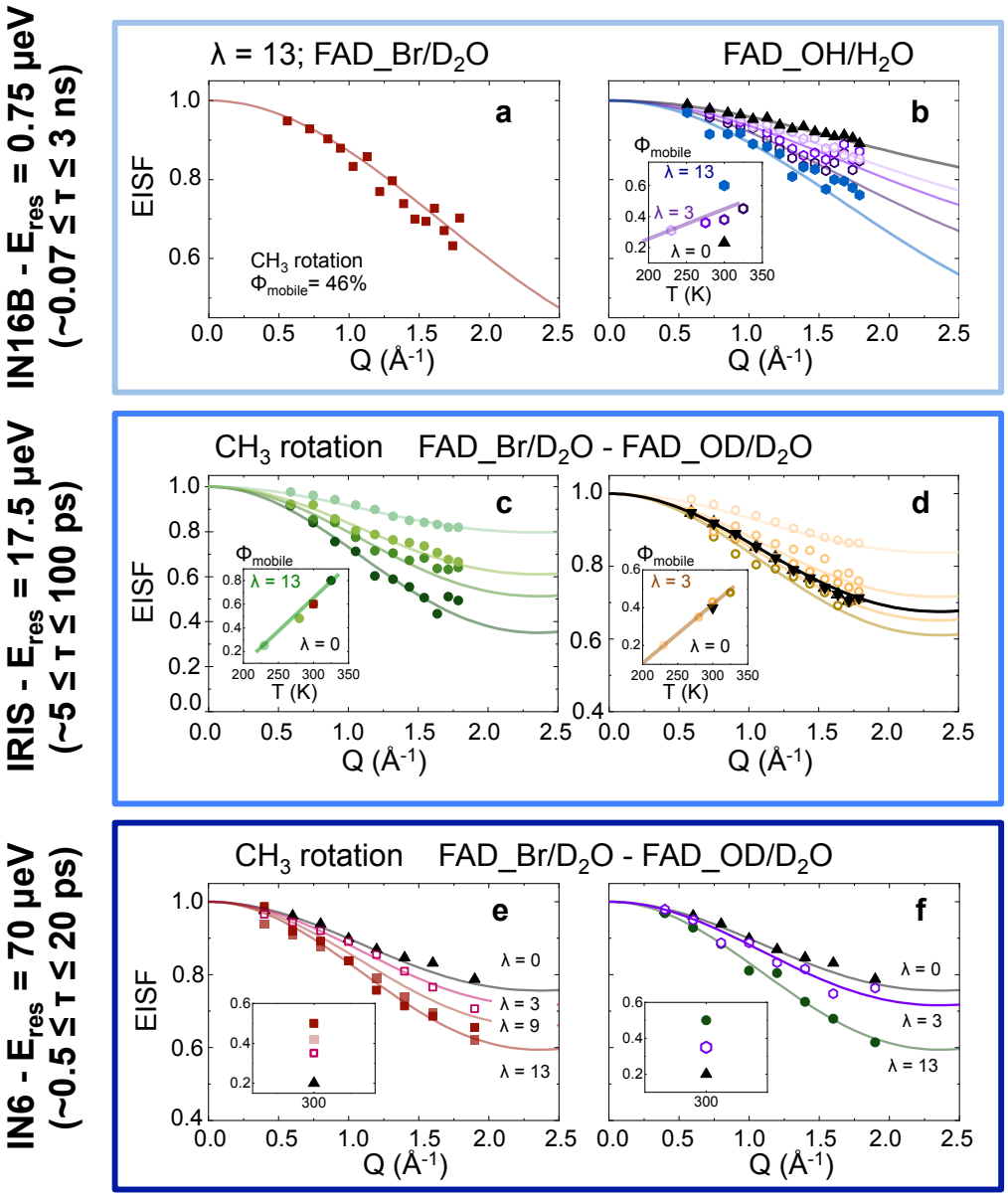

Supplementary Figure 15 | Elastic Incoherent Structure Factor (EISF). a, Br-form D_2O-hydrated, at λ=13 (300 K; E_{res}=0.75 μeV). EISF was modeled considering methyl rotation. **b**, OH-form, H_2O-hydrated (E_{res}=0.75 μeV), at λ=0 (300 K); 3 (from 230 to 325 K) and 13 (300 K). EISF was modeled considering OH^- hopping. **c**,**d**, OD-form, D_2O-hydrated, at λ=3 and 13 (from 230 to 325 K; E_{res}=17.5 μeV). EISF was modeled considering methyl rotation. **e**,**f**, Br- and OD-form, D_2O-hydrated at $0 \leq \lambda \leq 13$ (300 K; E_{res}=70 μeV). EISF was modeled considering methyl rotation.

Supplementary Table 5: Mobile fraction from EISF modelling. Data have been modelled according to equations (12 and 13a-b). Fractions as modelled according to polymer unit (considering aminated poly(phenylene oxide) as backbone [2,4] and quaternary ammonium (QA) as a polymer side group; Fig. 1c main paper) and water uptake for $3 \leq \lambda \leq 13$.

E_{res} (μeV)	Composition	T (K)	λ	Movement	Mobile fraction
0.75	OH/H_2O	300	0	OH^- hopping	0.23 ± 0.06
		230	3		0.31 ± 0.03
		275			0.36 ± 0.04
		300			0.38 ± 0.04
		325			0.45 ± 0.04
		300	13		0.60 ± 0.03
	Br/D_2O	300	13	Methyl rotation	0.55 ± 0.05
17.5	Br/D_2O	300	0	Methyl rotation	0.40 ± 0.04
					0.42 ± 0.05
		230	3		0.20 ± 0.02
		280			0.35 ± 0.03
		300			0.43 ± 0.04
		325			0.48 ± 0.05
	OD/D_2O	230			0.25 ± 0.02
		280			0.48 ± 0.05
		300	13		0.60 ± 0.06
		325			0.80 ± 0.08
	Br/D_2O	300			0.60 ± 0.05
70	Br/D_2O	300	0	Methyl rotation	0.32 ± 0.04
	OH/H_2O				0.33 ± 0.06
	OH/H_2O	230	3		0.28 ± 0.03
					0.35 ± 0.03
		300	7		0.39 ± 0.04
	Br/D_2O		9		0.42 ± 0.04
	OD/D_2O		13		0.50 ± 0.05
					0.52 ± 0.04

2.4. Dispersive QENS signal and translational diffusion of water molecules

Our QENS profiles were analyzed using the model for water dynamics suggested by Sears [49, 53-55], which refers to the center of mass motions of the molecular or ionic species (H_2O, OH^-) that are dominated by the heavy O atom, probed by scattering from the ^1H nuclei. Within the context of this model applied to aqueous media, the narrow Lorentzian component is associated with *Q*-dependent translational diffusion of the mobile species, while the broader component reflects a convolution of translational and rotational or pseudo-rotational contributions [49, 53-55].

Self-diffusion coefficients (D_{tr}) for translationally mobile H_2O/OH^- species were evaluated by plotting the HWHM (Γ_{tr}) of the narrow Lorentzian component *vs* Q^2 and fitting the data using a jump model between sites separated by an average distance (l) with a mean residence time (τ_0) during which the molecules undergo oscillatory motions:

$$\Gamma_{tr} = \frac{D_{tr}Q^2}{D_{tr}Q^2\tau_0+1} \quad (14)$$

Information about the rotational relaxation time ($\tau_{rt}=\hbar/\Gamma_{rt}$) is obtained from the linewidth of the broad Lorentzian component ($\Gamma_{tr}+\Gamma_{rt}$; representing a convolution of translational and rotational contributions within the Sears model described above).

While modelling the data this fast component was not taken into account as comparable to the polymer side-chain relaxation (a few ps). It would have been theoretically detectable in the isotopic subtraction performed to highlight the water dynamics within the polymer metrics (OH/H_2O – OD/D_2O; where OD/D_2O accounts fro the polymer dynamics in its swollen state); however, as consequence of the low statistics (due to propagation of the error while performing the subtraction) did not allow evaluating this fast component.

Supplementary Table 6: Water translational dynamics modelled according to equation (14). Activation energy (E_A) was computed according to $D = A\ Exp\ (-E_A/RT)$. D_{lr} relates to the long-range dynamics as detected by the analysis of the intermediate scattering function (Supporting Text 2.5).

E_{res} (μeV)	Contrast	T (K)	λ	$D_{tr} \times 10^{-5}$ ($cm^2\ s^{-1}$)	$D_{lr} \times 10^{-5}$ ($cm^2\ s^{-1}$)	τ_0 (ps)	E_A (kJ mol^{-1})
		300	13		0.33 ± 0.04		
		280	13	0.90 ± 0.05		2.6 ± 0.4	
17.5	OH/H_2O	300	13	2.30 ± 0.04	-	1.4 ± 0.2	24.5 ± 4.5
		325	13	3.90 ± 0.05		0.9 ± 0.2	
			7	1.12 ± 0.04		3.4 ± 0.3	
70	OH/H_2O	300	9	1.73 ± 0.03		2.2 ± 0.2	
			13	2.04 ± 0.05	-	1.5 ± 0.1	

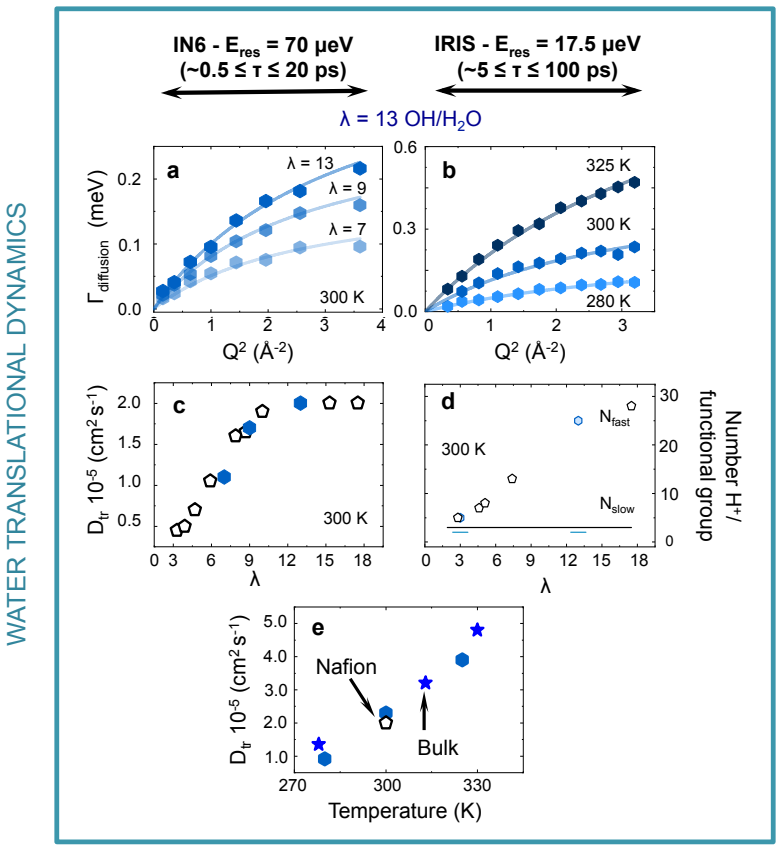

Supplementary Figure 16 | Translational diffusion for FAD-55 at 7≤*λ*≤13; 17.5≤E_{res}≤70 μeV. a,**b**, D_{tr} for OH-form, H_2O-hydrated, as function of water uptake (7≤*λ*≤13, at 300 K; **a**) as well as temperature (280≤*T*≤325 K, at *λ*=13; **b**). Data have been acquired at E_{res}=70 (**a**) and 17.5 μeV (**b**). **c,** Comparison between water translational diffusion within FAD (blue symbols) and Nafion (black symbols [23]) membrane. **d**, Comparison between water translational diffusion within FAD (fully hydrated; dark blue filled symbols are related to OH/H_2O sample; light blue filled symbols are related to OH/H_2O – OD/D_2O sample), Nafion (black symbols [23]) membrane and bulk water (star symbols [53,56]). **e**, Comparison between the relative population of slow- and fast-moving species within FAD (OH/H_2O; blue symbols) and Nafion (black symbols [23]) membrane. Data have been computed using equation (14).

Comparison between datasets obtained at IN6-Sharp and IRIS (Supporting Figs. 16a-b; respectively), reveal good reproducibility of the modelled parameters, which also overlap quite well with the data presented for Nafion (Supporting Fig. 16d). From the data at high resolution, as previously discussed, it was also possible to model a long-range diffusion (Supporting Fig. 16c), which is slowed down with respect to Nafion (Supporting Fig. 16e). Globally the analysis suggests that at *λ*=13 water trapped into the polymeric matrix behaves as bulk water (Supporting Fig. 16f). The analysis indicates that similarly to Nafion, there are two populations, one fast and one slow (Supporting Fig. 16g).

2.5. OH^- hopping and its coupling with water dynamics

To disentangle these contributions, we analyzed the intermediate scattering function ($I(Q, t)$) over the entire investigated timescale at all instruments, and modeled it according to both polymer relaxation and hydrating medium dynamics. We then decoupled ion-hopping from the water diffusion by accounting for the relative populations of protons involved in each motion as [24]:

$$\mathrm{I(Q,t)} = \mathrm{Amp}\left[\Phi_P I_P(Q,t) + \Phi_W\left(\mathrm{N}_{slow} I_{w_{slow}}(Q,t) + \mathrm{N}_{fast} I_{w_{fast}}(Q,t)\right)\right]\mathrm{R(t)} \quad (15)$$

Here, $R(t)$ is the normalized (i.e. to $R(0) = 1$) inverse Laplace-Fourier transform of the energy resolution function as determined by the sample at 2 K, Amp is an arbitrary amplitude function corresponding to the neutron counting rate scaling, Φ_P and Φ_W are the fractions of polymer and water in the mixture, $I_P(Q,t)$ is the contribution of the polymer matrix, $I_{w\,fast}(Q,t) = I_{loc}(Q,t) \times I_{lr}(Q,t)$ and accounts for localized and long-range dynamics, while N_{fast} and N_{slow} are the number of mobile protons involved in the fast (H_2O) and slow (OH^-) dynamics, respectively.

The intermediate scattering function of each component is modeled according to a simple exponential function:

$$\Phi(\mathrm{t}) = \exp\left[-\left(\frac{t}{\tau}\right)\right] \quad (16)$$

Supplementary Table 7: Parameters used to model $I(Q,t)$ according to equations (15-16). The fractions are modelled assuming the polymer unit to be aminated poly(phenylene oxide as backbone [2,4] with a quaternary ammonium as the side group; Fig. 1c main paper), with water uptake between $3 \leq \lambda \leq 13$, and computed using the intensity of the exponential function at $\lambda=0$. Error on τ_w is on the order of 10%.

λ	Dynamics	Fraction	Mobile species
0	Polymer	0.86	-
	Hopping	0.14	-
3	Polymer	0.7	-
	Fast water	0.3	5
	Slow water		2
13	Polymer	0.3	-
	Fast water	0.7	25
	Slow water		2

After an initial decay, samples with low hydration (λ=0,3) levels first develop a plateau followed by a shallower *I(Q,t)* reduction at longer times (Supplementary Figs. 16a-b). This is particularly visible at 230 K (Supplementary Figs. 17b,e,h,k). Under fully hydrated conditions (λ=13; Supplementary Fig. 17c), diffusional processes dominate, as clearly evidenced by the *Q*-dependence of *I(Q,t)* (Supplementary Figs. 17f,i,l). Data in time domain have been modelled according to equations (15 and 16), and a direct correlation between time and energy domain is observed. An attempt to model the *I(Q,t)* using a combination of exponential (for water) and stretched exponential functions (for polymer; $\Phi_{KWW}=exp[-(t/\tau_w)^{\beta}]$; where τ_w is a characteristic relaxation time and β is a stretching parameter) required $0.7 \leq \beta \leq 0.9$.

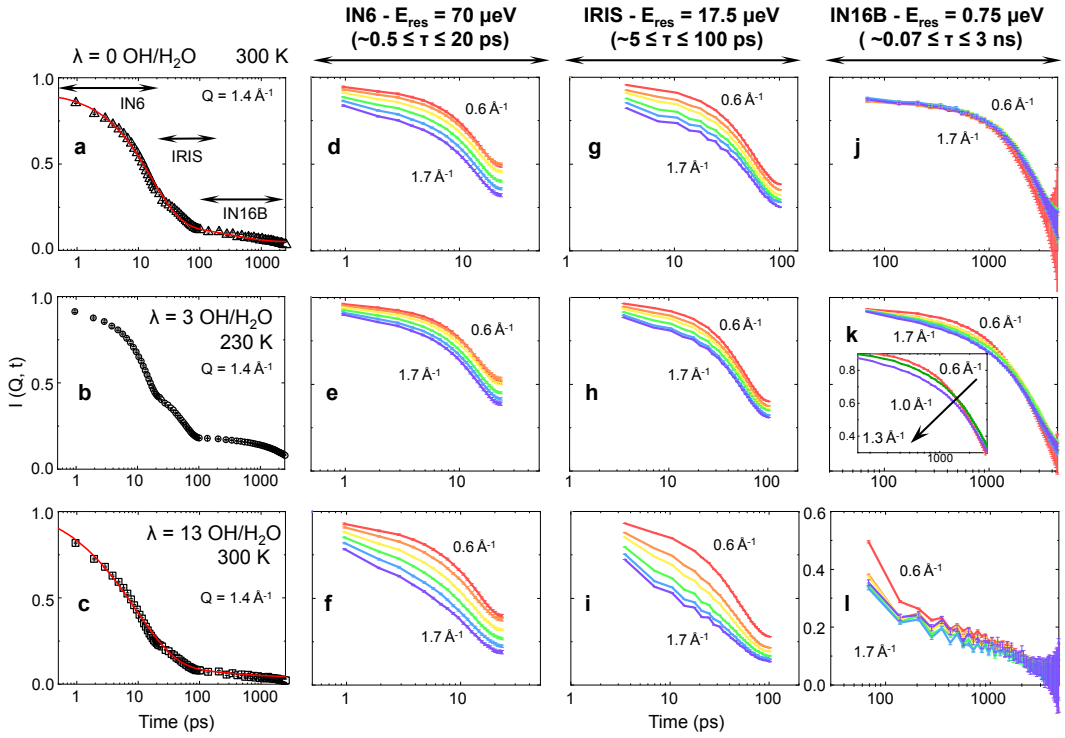

Supplementary Figure 17| Intermediate scattering function. a-c, Scattering profiles in the time domain for dry (λ=0; **a**) and H_2O-hydrated (λ=3,13; panels **b**,**c**) OH samples, at 230 K and 300 K; *Q*=1.4 $Å^{-1}$. The global fit (red continuous curve) is overlaid on the data points (black). **d-l**, *Q*-dependency of the *I(Q,t)* over the investigated timescales (IN6-Sharp - E_{res}=70 μeV- panels **d-f**; IRIS - E_{res}=17.5 μeV- panels **g-i**; IN16B - E_{res}=0.75 μeV- panels **j-l**). The inset in panel **k** is to show the deviation from the quadratic dependence of the intermediate scattering function for OH/H_2O sample at λ=3 and *T*=230 K in the nanosecond timescale.

Data in time-domain (λ=13) highlight the presence of a long-range diffusional of around one order of magnitude slower that D_{tr} (Supplementary Table 6).

To summarize, striking features of our QENS analysis are, on one hand, the presence of ultra-slow OH^- back-and-forth hopping similarly to H_3O^+ in Nafion, and on the other hand, the delayed establishment of long-range translational diffusion, as 7 water molecules per ionic group are needed to reach highly connected efficient transport in the anionic membrane while H_2O translation occurred down to low (λ~3) hydration values in Nafion [23].

Supplementary Text 3.
Structural and chemical studies
Small and Wide angle neutron and X-ray scattering profiles, as well as FTIR profiles were acquired for FAD H_2O-hydrated in OH- and Cl-form before and after treatment in oven at T=40 °C. The two ionic forms have been chosen to best compare structure with ionic conductivity.

3.1. SANS – SAXS/WAXS investigation
Scattering profiles were all acquired in a sealed quartz cuvette for: i) dried membranes after exposing the sample to ambient humidity (e.g. λ~3), and ii) after pad drying the excess of surface water in membranes previously immersed in liquid H_2O (e.g. λ~13). The raw SANS data were processed using the Mantid framework [50] following the standard procedures for the instrument (detector efficiencies, measured sample transmissions, absolute scale using the scattering from a standard polymer, etc.) [57].

The comparison between SANS profiles at low hydration for the two ionic forms (OH^- and Cl^-; black and pink symbols in Supplementary Fig. 18a), suggests no evident degradation, as the two profiles are completely superimposable. At high hydration SANS profiles for the two ionic forms (OH^- and cl^-; blue and brown symbols in Supplementary Fig. 18b), suggest similar large-scale structure, as the two profiles are have similar behaviour at low-Q. Small differences are found at high-Q, where the SANS profile for Cl-form seems suggesting the presence of ionomer peak.

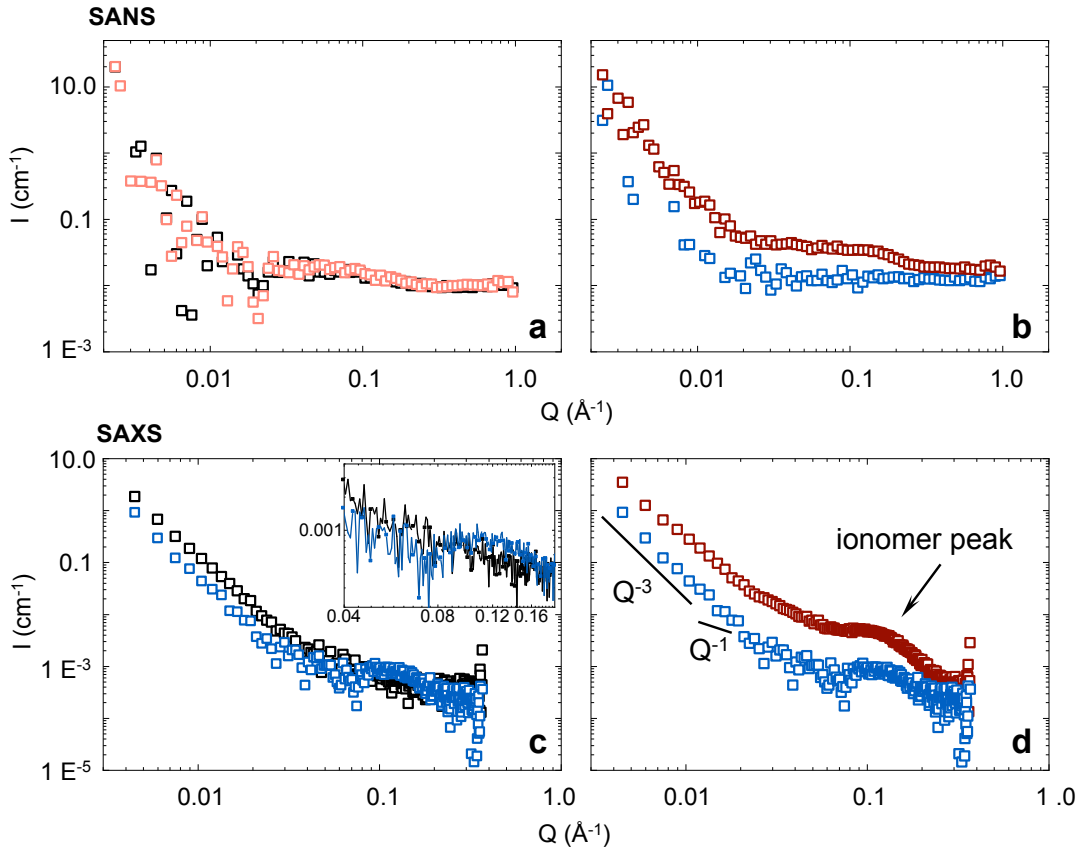

Supplementary Figure 18| Small Angle Neutron and X-Ray Scattering (SANS and SAXS). Scattering profiles were recorded for dried sample rehydrated at room humidity (λ~3); black and pink symbols for OH- and Cl-form, respectively) and fully hydrated (λ~13; blue and brown symbols for OH- and Cl-form, respectively). **a**-**b**, SANS profiles; **c**,**d**, SAXS profiles. Profiles were recorded at room temperature.

The comparison between SAXS data for OH-form in its partially (dried sample exposed to room humidity; black symbols) and fully hydrated (blue symbols; Supplementary Fig. 18c) reinforces the presence of some porosity within the polymer matrix. Not surprisingly, the ionomer peak (Q~0.11 Å^{-1}; $d=(2\pi/Q)$~5.6 nm; Supplementary Figs. 18c-d) becomes defined only in the fully hydrated state, as previously seen for Nafion [58]. This figure agrees with the estimate of pore size as detected using AFM (Supplementary Fig. 21). At low-Q, SAXS profiles for hydrated membranes seem to be best described by a Q^{-3} power-law term, possibly due to the correlation between water clusters and the lamellar stacks. An additional narrow Q^{-1} power-law term may be identified in the SAXS profiles, suggesting the presence of some one-dimensional structures in the sample (possibly rod-like [59-60]; Supplementary Fig. 18d).

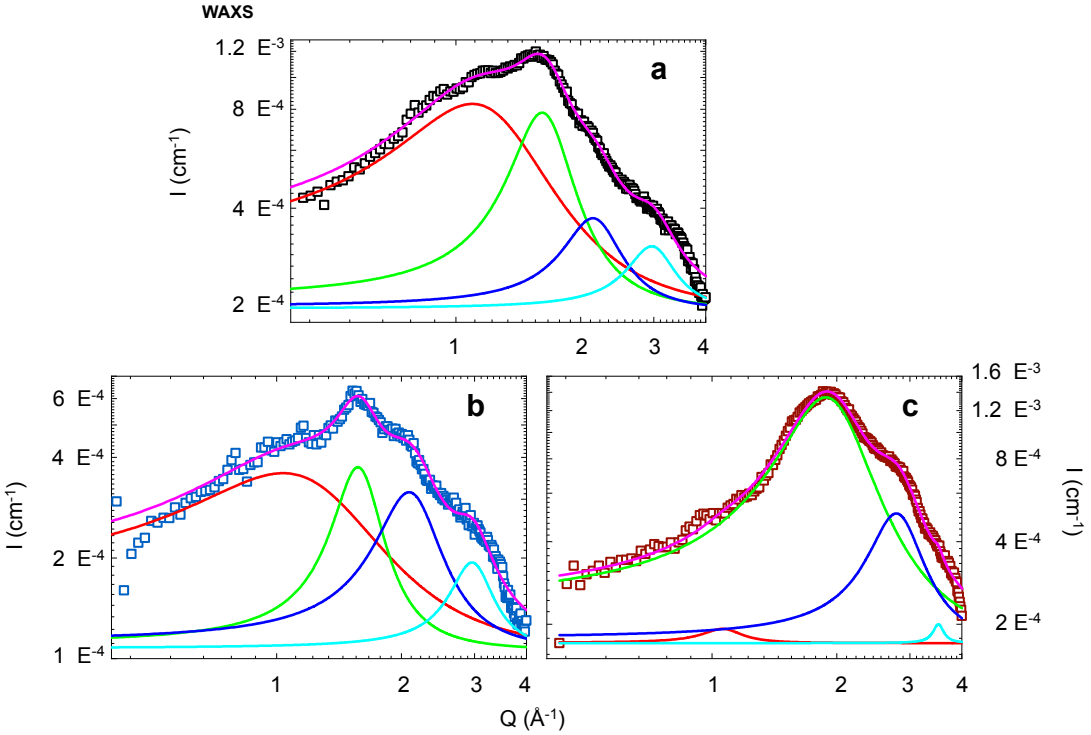

Supplementary Figure 19| Wide Angle X-Ray Scattering (WAXS). a-c, Scattering profiles for partially (dried sample exposed to room humidity; black symbol, OH-form) and fully hydrated (blue and brown symbols for OH- and Cl-form; respectively). The entire sets of scattering profiles were analyzed using a combination of pseudo-Voight functions.

WAXS profiles (Supplementary Fig. 19) have been modeled using a combination of four contributions, based on the shape of the raw data. The first peak is centered at around 1.06 $Å^{-1}$; the second one around 1.60 $Å^{-1}$ in the OH-form and shifts at ~1.90 $Å^{-1}$ in Cl-form. Similarly the third peak, centered at ~2.10 $Å^{-1}$ in the OH- form, shifts to ~2.80 $Å^{-1}$ in the Cl-form. Beside the shift at higher Q, these two latter peaks are almost one order of magnitude more intense in the Cl-form, in respect to the OH-form, suggesting that are related to the ion (OH *vs* Cl). The last peak, despite having similar intensity in all three samples, seems again slightly shifted in the Cl-form (3.0 *vs* 3.5 $Å^{-1}$).

3.2. FTIR investigation

The comparison between IR profiles for FAD in its OH- and Cl-form at room humidity (e.g. λ~3; Supplementary Fig. 20), does not highlight any major change in frequencies, and therefore suggest no degradation at low hydration. Not unexpectedly the signal just above 1600 cm^{-1} appears broader in the OH-form.

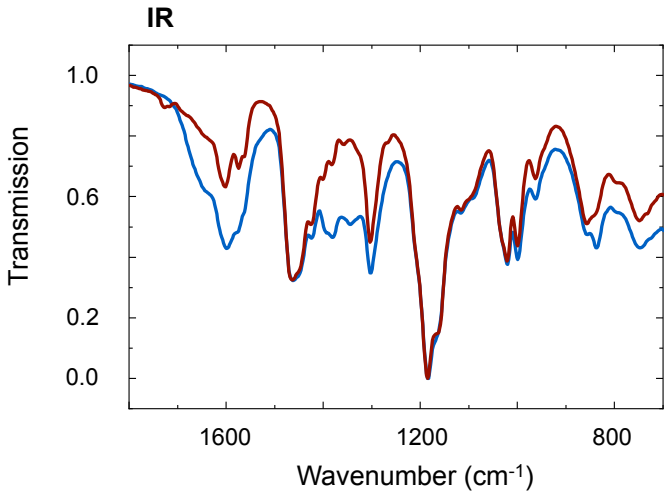

Supplementary Figure 20 | Fourier Transform Infrared (FTIR) spectroscopy. Comparison between profiles for partially hydrated (room humidity; λ~3) membrane in OH- (blue line) and Cl-form (brown line).

3.3. AFM imaging

AFM images were recorded on Bruker Dimension Icon with SNL-10A and Scanasyst fluid+ probe (both with nominal tip radius: 2 nm, resonance frequency: 65 kHz and spring constant: 0.35 N m^{-1}) with scan rate 0.5 Hz and 512 scans per line. Membrane samples were allowed to equilibrate at ambient humidity and temperature for 24 h (λ=3, OH- and Cl-form; Supplementary Figs. 21a-b, respectively), and imaged in tapping mode. Phase measurements were conducted at the same time as the morphology was mapped. Sample imaging in water for Cl-form (Supplementary Fig. 21c) was carried out using PeakForce tapping mode. The images were analysed by Nanoscope Analysis software.

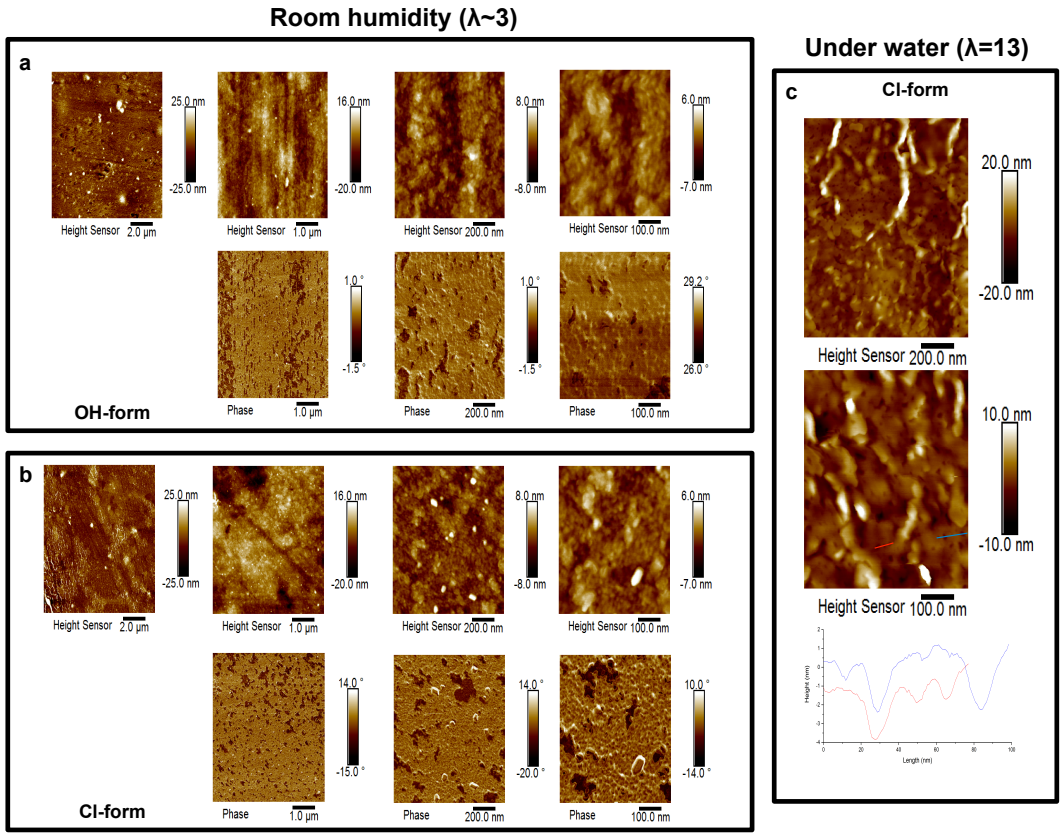

Supplementary Figure 21 | Atomic Force Microscopy (AFM) imaging. a-**b**, Comparison between profiles for partially hydrated (room humidity; λ~3) membrane in OH- (**a**) and Cl-form (**b**). **c**, Profiles recorder in fully hydrated state (λ=13) for FAD in Cl-form.

References

49. Bée, M. *Quasielastic Neutron Scattering: Principles and Applications in Solid State Chemistry, Biology and Material Science*. (Adam Hilger, Bristol, 1988).
50. O.Arnold, O. et al. Mantid - Data analysis and visualization package for neutron scattering and μSR experiments. Nucl. Instrum. *Methods Phys. Res. Sect. A* **764**, 156-166 (2014).
51. Azuah, R. T. et al. DAVE: A comprehensive software suite for the reduction, visualization, and analysis of low energy neutron spectroscopic data. *J. Res. Natl. Inst. Stand. Technol.* **114**, 341-358 (2009).
52. Pruppacher, H. R. Self-diffusion coefficient of supercooled water. *J. Chem. Phys.* **56,** 101-107 (1972).
53. Teixeira, J., Bellissent-Funel, M.-C., Chen, S.H. & Dianoux, A.J. Experimental determination of the nature of diffusive motions of water molecules at low temperatures. *Phys. Rev. A* **31,** 1913-1917 (1985).
54. Sears, V. F. Theory of cold neutron scattering by homonuclear diatomic liquids: I. Free rotation. *Can. J. Phys.* **44,** 1279-1297 (1966).
55. Sears, V. F. Theory of cold neutron scattering by homonuclear diatomic liquids: II. Hindered rotation. *Can. J. Phys.* **44,** 1299-1311 (1966).
56. Prielmeier, F. X., Lang, E. W., Speedy, R. J. & Lüdemann, H. D. The pressure dependence of self diffusion in supercooled light and heavy water, *Ber. Bunsenges Phys. Chem.* **92,** 1111-1117 (1988).
57. Heenan, R.K., Penfold, J. & King, S.M. SANS at pulsed neutron sources: present and future prospects. *J. Appl. Crystallogr.* **30**, 1140-1147 (1997).
58. Fumagalli, M. et al. Fast water diffusion and long-term polymer reorganization during Nafion membrane hydration evidenced by time-resolved small-angle neutron scattering, *J. Phys. Chem. B* **119**, 7068-7076 (2015).
59. Song, J.-M., Ko, B.-S., Young, J.-Y., Nho Y. C. & Shin J. A study on the morphology of polystyrene-grafted poly(ethylene-alt-tetrafluoroethylene) (ETFE) films prepared using a simultaneous radiation grafting method, *Radiat. Phys. Chem.* **97**, 374-380 (2014).
60. Zhao, Y. et al. Imidazolium-based anion exchange membranes for alkaline anion fuel cells: elucidation of the morphology and the interplay between the morphology and properties, *Soft Matter* 12, 1567-1578 (2016).